



Multi-proxy reconstructions of May–September precipitation field in China over the past 500 years

Feng Shi^{1,2}, Sen Zhao^{3,4}, Zhengtang Guo^{1,5,6}, Hugues Goosse², and Qiuzhen Yin²

¹Key Laboratory of Cenozoic Geology and Environment, Institute of Geology and Geophysics, Chinese Academy of Sciences, Beijing, 100029, China

²Georges Lemaître Centre for Earth and Climate Research, Earth and Life Institute, Université catholique de Louvain, Louvain-la-Neuve, 1348, Belgium

³Key Laboratory of Meteorological Disaster of Ministry of Education, and College of Atmospheric Science, Nanjing University of Information Science and Technology, Nanjing, 210044, China

⁴School of Ocean and Earth Sciences and Technology, University of Hawaii at Mānoa, Honolulu, HI 96822, USA

⁵CAS Center for Excellence in Tibetan Plateau Earth Sciences, Beijing, 100101, China

⁶University of Chinese Academy of Sciences, Beijing, 100049, China

Correspondence: Feng Shi (shifeng@mail.iggcas.ac.cn)

Received: 6 January 2017 – Discussion started: 16 January 2017

Revised: 21 October 2017 – Accepted: 15 November 2017 – Published: 22 December 2017

Abstract. The dominant modes of variability of precipitation for the whole of China over the past millennium and the mechanism governing their spatial structure remain unclear. This is mainly due to insufficient high-resolution proxy records of precipitation in western China. Numerous tree-ring chronologies have recently been archived in publicly available databases through PAGES2k activities, and these provide an opportunity to refine precipitation field reconstructions for China. Based on 479 proxy records, including 371 tree-ring width chronologies, a tree-ring isotope chronology, and 107 drought/flood indices, we reconstruct the precipitation field for China for the past half millennium using the optimal information extraction method. A total of 3631 of 4189 grid points in the reconstruction field passed the cross-validation process, accounting for 86.68 % of the total number of grid points. The first leading mode of variability of the reconstruction shows coherent variations over most of China. The second mode is a north–south dipole in eastern China characterized by variations of the same sign in western China and northern China (except for Xinjiang province). It is likely controlled by the El Niño–Southern Oscillation (ENSO) variability. The third mode is a “sandwich” triple mode in eastern China including variations of the same sign in western China and central China. The last two modes are reproduced by most of the six coupled climate models’

last millennium simulations performed in the framework of the Paleoclimate Modelling Intercomparison Project Phase III (PMIP3). In particular, the link of the second mode with ENSO is confirmed by the models. However, there is a mismatch between models and proxy reconstructions in the time development of different modes. This mismatch suggests the important role of internal variability in the reconstructed precipitation mode variations of the past 500 years.

1 Introduction

High-resolution regional paleoclimate field reconstructions are able to accurately reproduce the fine spatiotemporal structure of regional climate change on multiple timescales for the period prior to instrumental records. Such reconstructions are an essential source of information to document the climate variability at decadal to centennial timescales and can be used to assess the ability of climate models to simulate past climate change.

In order to obtain such a reconstruction of regional paleoclimate fields, dense proxy records and an adequate reconstruction method are required. Consequently, climate field reconstructions for the past millennium have focused mainly on regions for which abundant multi-proxy records are avail-

able, including Europe (Luterbacher et al., 2004), North America (Cook et al., 2004) and East Asia (Shi et al., 2015a). The primary types of proxy records are often tree-ring records and historical documents, mainly because of the data availability and their accurate dating, annual resolution, and demonstrable relationships with instrumental climate data (Fritts, 1976; Zhang, 1991). Other proxy records (e.g. ice core, coral, and varved sediment) have also been introduced into regional climate field reconstructions (e.g. Neukom et al., 2011), but they generally represent a small percentage of the data available in global compilations (e.g. PAGES 2k Consortium, 2013).

The reconstruction targets are generally temperature and temperature-related variables. Reconstructions of the precipitation field or other variables related to precipitation are less frequent (Cook et al., 1999; Casty et al., 2005; Neukom et al., 2013; B. I. Cook et al., 2015; Seftigen et al., 2015) because they require denser proxy networks than for temperature. Nevertheless, the Palmer Drought Severity Index (PDSI) has been reconstructed recently over the past millennium in North America (North American Drought Atlas, NADA; Cook et al., 1999), in Asia (Monsoon Asia Drought Atlas, MADA; Cook et al., 2010), in Europe (Old World Drought Atlas, OWDA; E. R. Cook et al., 2015), and in Oceania (Australia and New Zealand summer drought atlas, ANZDA; Palmer et al., 2015) using tree-ring records. All these datasets are available at the website of the National Oceanic and Atmospheric Administration (NOAA) (<https://www.ncdc.noaa.gov/data-access/paleoclimatology-data/datasets/climate-reconstruction>) and are widely used to identify the variability of droughts and pluvials over the past millennium (e.g. B. I. Cook et al., 2015).

The paleoclimate reconstruction methods are divided into climate index reconstruction (CIR) and climate field reconstruction (CFR) according to the reconstruction target. The CIRs are generally derived from either direct regression or indirect regression (Christiansen and Ljungqvist, 2017). Methods using the climate variables as the predictands (or dependent variable) and the proxies as the predictors (or independent variable) are called direct regression. In contrast, using the climate variables as the predictors and the proxies as the predictands leads to indirect regression. The composite plus scale (CPS) method is a widely used, classic direct regression that composites a group of proxy records using uniform or proxy-dependent weighting. The time series obtained is then scaled to have the same variance as the targeted regional or hemispheric averaged variable over a chosen interval. More generally, the regression process is usually based on some forms of univariate or multivariate linear regression and the regression parameters are estimated using classic methods – e.g. ordinary least squares, total least squares, variance matching. However, the problem is generally ill-posed because of the limited number of samples in the calibration period, and regularized methods have to be intro-

duced – such as the truncated principal component regression (truncated-PCR) (Mann et al., 1999), the regularized expectation maximization (RegEM) (Mann et al., 2008), and the Least Absolute Shrinkage and Selection Operator (LASSO) (McShane and Wyner, 2011).

The local (LOC) method is a promising method based on indirect regression. In the LOC method, each proxy record should be first calibrated using the local instrumental climate data, and the time series are then averaged to obtain the large-scale mean climate index (Christiansen, 2011). An indirect regression is used for the local calibration, justified by the fact that the proxy records are functions of climate variables and not the opposite. The reconstructions based on the LOC method are assumed to better preserve the low-frequency climate signal compared to other methods, though they would overestimate the high-frequency signal (Christiansen and Ljungqvist, 2011). The biases are partially corrected by the arithmetic mean of the regression coefficients of the linear regression and the inverse regression in the optimal information extraction (OIE) method (Shi et al., 2012). The hypothesis in the OIE method is that the regression coefficients are random variables with normal distribution that vary in the range provided by the classic linear regression and inverse regression. Additional methods have also been proposed recently to take into account some of the biases of classical methods based on regression such as the pairwise comparison (Hanhijärvi et al., 2013) or Bayesian method of various levels of complexity (e.g. Tingley and Huybers, 2010).

The CFR methods can be divided into the reduced space objective analysis-based method (Evans et al., 2001) and the point-to-point regression-based (PPR-based) method (Cook et al., 1999). A typical example of the first group of methods is provided by the study of Mann et al. (2009). The dominant empirical orthogonal function (EOF) patterns are first calculated from instrumental climate data. Their time coefficients are then estimated over the pre-instrumental data using a network of proxy records. Finally, the climate field over the pre-instrumental data is obtained by performing the product of the reconstructed time coefficients and the instrumental dominant EOF patterns. The underlying hypothesis is that the primary spatial modes of climate change during the instrumental period also explain a large fraction of the variability in the past. The advantage of this assumption is that only a few proxy records with sparse spatial coverage can be enough to reconstruct a climate field (Neukom et al., 2011). However, the EOF patterns discarded after EOF truncation include some information that is lost, leading to some uncertainties on a small spatial scale. For instance, the global temperature field reconstruction of Mann et al. (2009) was not consistent with a regional temperature field reconstruction in the western Qinling Mountains, China (Yang et al., 2013b). In addition, this method is not well adapted for reconstructions of precipitation field because of the high spatial heterogeneity of this variable (Gómez-Navarro et al., 2015).

The PPR-based method reconstructs the target variable at each grid point using a linear regression – e.g. PCR (Cook et al., 1999), RegEM regression (Shi et al., 2015a) or the OIE method (Yang et al., 2016) – by searching adequate proxy records among the ones available near the grid point. The goal of the PPR-based method is to maximize the retention of spatial information, but this method requires a sufficient number of suitable proxy records. Selecting only one type of proxy record, with the associated limited spatial distribution, may thus hinder the field reconstruction of precipitation (or of a variable sensitive to precipitation) for a large-scale region using the PPR-based method. For example, the tree-ring-based reconstruction of the MADA provides significant insights into past drought patterns in eastern Asia (Cook et al., 2010), but it performs poorly in reproducing dryness and wetness in eastern China because it only incorporates data from one short tree-ring width chronology from eastern China. Consequently, it would be invalid to extrapolate objective gridded drought variability on the basis of remote tree-ring records in western China (Yang et al., 2013a). Thus, a good option to obtain a regional pattern of precipitation is to use a PPR-based method in conjunction with multi-proxy records with good spatial coverage.

In eastern China, there are abundant historical records of precipitation variability (e.g. Zhang et al., 2003b; Zheng et al., 2006; Hao et al., 2016). Recently, numerous tree-ring records in western China and surrounding regions have been archived in published databases (Yang et al., 2014b; PAGES 2k Consortium, 2017). This offers an excellent and timely opportunity to integrate the data from tree-ring records from western China and historical records in eastern China to reconstruct the precipitation field for the whole of China. Feng et al. (2013) reconstructed the precipitation field in East Asia using multi-proxy records that reflect the variability in precipitation (e.g. Liu et al., 2016). However, the distribution of proxy records in western China was not sufficiently dense in that reconstruction. In addition, spatial information may have been partially lost using the EOF-based method mentioned above. This is a limitation for developing a further understanding of the dominant patterns of precipitation for the period before instrumental records and their possible driving mechanisms. In this work, we have incorporated additional tree-ring records from western China compared to previous studies and used the PPR-based framework with the OIE method to reconstruct the precipitation fields for China. Using this reconstruction, we then explore the dominant patterns of precipitation variability before the instrumental period and discuss their possible origin.

2 Data and methods

To reconstruct the precipitation field, we used a gridded instrumental precipitation dataset, proxy records that can be significantly related to precipitation in the domain studied,

and the OIE precipitation field reconstruction method. Other datasets were used to validate the reconstruction and explore possible driving mechanisms.

2.1 Instrumental data

Owing to the highly heterogeneous and localized variability in precipitation, the accuracy of regional precipitation estimates depends mainly on the spatial density of the stations (Wan et al., 2013). Thus, a dense distribution of datasets is considered as a priority.

We selected the China Ground Precipitation 0.5° longitude by 0.5° latitude Grid Dataset V2.0 (Zhao and Zhu, 2015), which is a monthly gridded precipitation dataset covering the period AD 1961–2010. This dataset is based on nearly all available national surface stations ($n = 2472$) in China. With the selected resolution, the whole of China includes 4189 grid points. The calibration period was set to AD 1961–1990 and the validation period was AD 1991–2000 for the reconstruction. We targeted precipitation data from the warm season (May–September, MJJAS) because historical documents mainly record variations in MJJAS precipitation.

Another instrumental precipitation dataset was used in this study to validate the reconstruction: the Homogenized Monthly Precipitation Dataset in China. It covers the interval 1900–2009 (Li et al., 2012), with a 5° longitude by 5° latitude grid resolution. This dataset includes data from all available national surface stations in China before AD 1960. The MJJAS mean precipitation anomaly for China for the interval AD 1920–1960 is selected here as an independent verification data. Some unusual values were evident for the period before AD 1920, as shown in original Fig. 12 of Li et al. (2012), and these are likely a result of the sparse distribution of observation points. The two datasets are both developed by, and available from, the National Meteorological Information Center, Chinese Meteorological Administration.

2.2 Tree-ring records

The use of tree-ring records has multiple advantages, including their annual resolution, easy replication, wide distribution, and significant corroboration from instrumental records. Consequently, such records are considered to be primary and practical archives for reconstructing precipitation fields and are widely used to reconstruct regional precipitation variability in China over the past half millennium (e.g. Shao et al., 2005; Yang et al., 2014b).

The candidate tree-ring records are required to satisfy three conditions: (1) all records must be archived in public repository; (2) each record needs to at least cover the period from AD 1875 to AD 1977; (3) if raw tree-ring width measurements are available, they must be based on at least five samples for each year to ensure good replication. The screened 372 chronologies include 371 tree-ring width chronologies and a tree-ring oxygen isotope chronology.

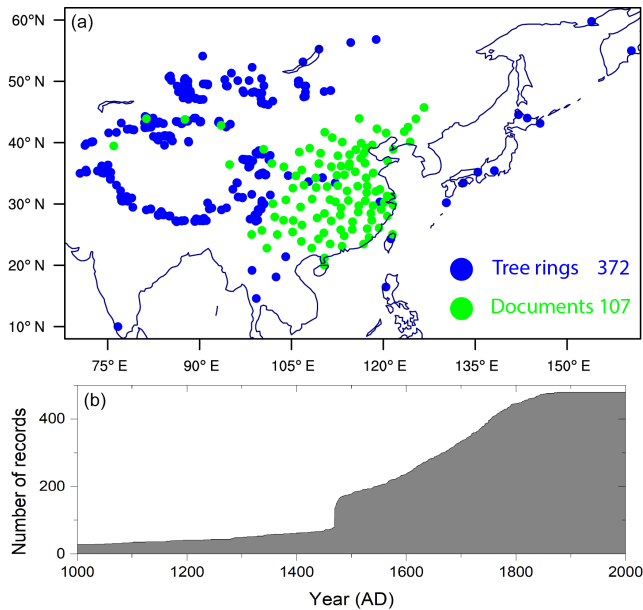


Figure 1. Map showing the locations of proxy records (a) and plot of the number of proxy records for each year (b).

To maximize the overlap lengths of the instrument data and proxy records, all tree-ring records were extrapolated to AD 2000 using the RegEM algorithm (Schneider, 2001). Here, the truncation parameters for the RegEM algorithm were set to the same values as used by Mann et al. (2008). A total of 197 of 372 tree-ring chronologies were extrapolated. The maximum and mean extrapolation lengths of the 197 chronologies were 23 and 11 years, respectively. The extrapolation bias was ignored because of the short extrapolation length.

We synthesized 372 tree-ring records from China and surrounding areas, as shown in Fig. 1. The tree-ring records are located mainly in 14 countries including Bhutan, China, India, Japan, Kazakhstan, Kyrgyzstan, Laos, Mongolia, Nepal, Pakistan, Philippines, Russian Federation, Thailand, and Vietnam. There are only very few tree-ring records in eastern China. This indicates that the currently available tree-ring records are not sufficient for reconstruction of the precipitation field in eastern China.

2.3 Dryness/wetness index (DWI)

In eastern China, abundant records of drought and flood conditions found in historical documents have been used to reconstruct past climate (Zhang, 1991; Ge, 2011; Hao et al., 2016). One of the most valuable examples is the Yearly Charts of Dryness/wetness (DWI) in China for the Last 500-Year Period dataset (Chinese Academy of Meteorological Science, 1981). The DWI dataset, also known as the drought/flood indices (DFI), provides essential information allowing for the assessment of precipitation variability in

eastern China (e.g. Wang and Zhao, 1979; Zhang, 1988; Qian et al., 2003a). This DWI dataset includes data from 120 locations that are distributed mainly in eastern China and north-eastern China, with a few in western China. Herein, 13 DWI are excluded because they cover too short time periods. The DWI for each year has five grade values: very wet (grade 1), wet (grade 2), normal (grade 3), dry (grade 4), and very dry (grade 5). The DWI dataset is mainly derived from the local chronicles and started from AD 1470 (the sixth year of the Chenghua reign in the Ming dynasty). It describes the onset, duration, areal extent, and severity of each drought or flood event in each province (Chinese Academy of Meteorological Science, 1981; Zhang, 1983). Experts, mainly from the provincial meteorological bureaux, the China Meteorological Administration, Peking University, and the Chinese Academy of Sciences, have converted the qualitative textual descriptions into quantitative data (Chinese Academy of Meteorological Science, 1981).

The reliability of DWI has been described in previous studies (Zhang, 1983, 1988). The homogeneity of DWI was demonstrated using the chi-square test (Zhang, 1983), and the reliability of DWI in terms of spatial pattern was verified through comparison with the eigenvectors of the instrumental precipitation during the period AD 1951–1974 (Wang and Zhao, 1979).

However, DWI records still have some weaknesses. Firstly, most of the DWI records are not continuous in time (Zhang, 1983), as illustrated in Fig. S1 in the Supplement for the 107 DWI records. The maximum (mean) number of missing values of 107 DWI records during the period AD 1470–2000 was 446 (157). Secondly, the DWI records are unevenly distributed over space. Figure S2 shows the location and number of DWI records during the period AD 1470–2000. In this figure, a value of “100” means that it has 100 observed values during the period AD 1470–2000. The figure indicates that 91 of 107 DWI records are located in eastern China (east of longitude 105° E), which is the economically developed region. There are only 16 DWI records west of longitude 100° E. Additionally, an uncertainty due to subjective judgment is unavoidable for the historical documentary, even though different sources have been used to cross-validate the final reconstruction (Zhang, 1983; Man, 2009; Ge, 2011; Zheng et al., 2014a). Moreover, the range of values is within five grades and the DFI record is not a direct precipitation value, which also limits the accuracy and ability to detect extreme events (Zheng et al., 2014a).

In order to improve the quality of the DWI dataset, Professor Zhang De'er led a team of scientists, that carried out research for 20 years to identify the weather events in China over the past 3000 years. This resulted in the publication of a book, entitled “A compendium of Chinese meteorological records of the last 3000 years”. Each record has been carefully cross-checked with more than 8000 historical documents (Zhang, 2004). However, the updated dataset has not been archived in a published repository so far.

This publicly available DWI dataset has been extended to AD 2000 using the annual average and standard deviation of observed rainy season precipitation (May–September, MJ-JAS) when the instrumental precipitation is available (Zhang and Liu, 1993; Zhang et al., 2003a). In this work, 85 DWI records need to be interpolated because of missing values. The RegEM method was also used to interpolate the DWI data based on their mutual covariance with the other available data. The maximum (mean) length for interpolation was 446 (157) years. Any interpolation bias was ignored, as the historical documentary data record a regional drought or flood event rather than a local phenomenon, and they show good regional spatial consistency.

2.4 Selected proxy records

In total, we assembled 479 proxy records, which included 371 tree-ring width chronologies, 1 tree-ring oxygen isotope chronologies, and 107 DWI records. Each record is required to be significantly correlated with one or more instrumental precipitation records at the 90 % ($p < 0.1$) confidence level during the overlap period, based on both raw data and linearly detrended data. Moreover, previous studies have repeatedly verified a significant relationship between tree-ring precipitation reconstructions and the DWI on a regional scale (e.g. Zhang, 2010). The common period to all of the proxy records is AD 1875–1977. The number of proxy records has a visible changing point from AD 1470 to AD 1469 after extrapolation/interpolation, with a 41.91 % decrease from 136 to 79. The details of each record are provided in Table S1 in the Supplement and Fig. 1.

2.5 El Niño–Southern Oscillation (ENSO) and Pacific Decadal Oscillation (PDO) indices

Two modes of natural climate variability, the El Niño–Southern Oscillation (ENSO) and Pacific Decadal Oscillation (PDO), are used to explore the possible connection between our reconstruction and large-scale variability, since those two modes have already been shown to affect precipitation in China on interannual, interdecadal, and multi-decadal timescales based on instrumental analysis (Huang and Wu, 1989; Ma, 2007; Qian and Zhou, 2014). Multiple ENSO and PDO reconstructions focused on the past millennium have been assembled in our previous work (Shi et al., 2017). Without loss of generality, we selected three reconstructed ENSO indices (Cook et al., 2008; McGregor et al., 2010; Li et al., 2013a) and three PDO indices (D’Arrigo et al., 2001; D’Arrigo and Wilson, 2006; Shen et al., 2006) that have good performance in relation to instrumental data. Note that three ENSO indices have a strongly significant relationship during the common period AD 1650–1977 with the range of correlation coefficients [0.58, 0.66, 0.84], but the three PDO indices are only very weakly related during their common period AD 1700–1979 with the range of correlation

coefficients [0.03, 0.09, 0.13]. As argued recently (e.g. Newman et al., 2016), the PDO cannot be considered as a single dynamical process, but a result of the combined influence of remote tropical forcing and local North Pacific atmosphere–ocean interactions. This makes it a particularly challenging target for proxy-based reconstructions, explaining the poor agreement between the available series.

2.6 Climate model simulation

Six coupled climate models were used to assess whether their past 1000 modelling experiments for the interval AD 850–1849 are consistent with our reconstruction. These are BCC-CSM1.1 (T. Wu et al., 2010), CCSM4 (Landrum et al., 2012), FGOALS-s2 (Man et al., 2014), GISS-E2-R (Schmidt et al., 2014), IPSL-CM5A-LR (Dufresne et al., 2013), and MPI-ESM-P (Jungclaus et al., 2010). A description of the six models, sponsoring institutions, and main references is given in Table S3 of Shi et al. (2015a). For details and data of the past 1000 experiments, see the websites of the Paleoclimate Modelling Intercomparison Project Phase 3 (PMIP3) and the fifth phase of the Coupled Model Intercomparison Project (CMIP5). All simulated results were interpolated to the same temporal and spatial resolution as the reconstruction in this study.

2.7 Reconstruction method

The OIE method has been successfully used to reconstruct the South Asian summer monsoon index over the past millennium (Shi et al., 2014), the northern hemispheric temperature over the past 2 millennia (Shi et al., 2015b), and the precipitation field over the past 500 years in the western Qinling Mountains, China (Yang et al., 2016). The drawback of this method is an overfitting tendency. An independent test data is needed for cross-validation to avoid it.

This method (version 1.3) within the PPR-based framework comprises three steps. The first step is to search for the candidate proxy records. We firstly selected all possible predictors with significant relation to the target. Then, we sorted them as a function of their descending distances from the predictor to the target. We excluded the predictors with distances more than 3500 km. We assumed that the predictor is unlikely to provide useful information about the precipitation variability at a grid point beyond 3500 km. As a result, four situations are possible. (1) The number of candidate predictors was more than five, and the first five predictors included at least one record that could reach AD 1470. This target was constructed using the first five predictors. Five is the initial minimum number of candidate predictors according to past experience (Cook et al., 2013). (2) The number of candidate predictors was more than five, but the first five predictors did not include any record that could reach AD 1470. We increased the number of predictors until a predictor could reach to AD 1470. The target was constructed using the se-

lected predictors, whose number was more than five. (3) The number of candidate predictors is more than five, but none could reach to AD 1470. We increased the number of predictors until we found the predictor with the maximum time span. (4) The number of candidate predictors is less than five but more than three. This means that this target cannot meet the requirement of replication, but we tolerate it and use all possible predictors to reconstruct it.

The second step is to determine the weighting for the proxy records using the correlation coefficient between the candidate proxy record and the reconstructed target according to Shi et al. (2014)'s method. The third step is regression of the proxy record using the ensemble LOC regression method (Shi et al., 2012).

Traditional accuracy and skill parameters, including the square of the Pearson product–moment correlation coefficient (r^2) between the reconstruction and the instrumental data during the verification period, the reduction of error (RE) in the verification period, and the coefficient of efficiency (CE) in the verification period (Cook et al., 2010), were used to evaluate the reliability of the reconstructions. The uncertainty was calculated using the standard deviation of the residual between the reconstructed and instrumental precipitation data during the verification period. Moreover, the Pearson's sample linear cross-correlations at lag 0 is used for the correlation analysis, and the significance of the correlation for the filtered time series was accessed using the effective number of degrees of freedom following Zhao et al. (2016).

2.8 Ensemble empirical mode decomposition and superposed epoch analysis

The ensemble empirical mode decomposition (EEMD) method (Huang and Wu, 2008; Wu and Huang, 2009) was used to analyse the reconstructed mean MJJAS precipitation time series for eastern China, western China, and the whole of China. Eastern and western China are simply divided along the longitude 105°. Following Mann et al. (1995), the interannual timescale was set to < 8 years. The interdecadal timescale was defined as ≥ 8 years and < 35 years. The multidecadal timescale was defined as ≥ 35 years and < 100 years, and the centennial scale was > 100 years.

Superposed epoch analysis is traditionally used to analyse the influence of volcanic eruption on the climate, e.g. Bradley (1988). Here, the code to compute superposed epoch analysis has been downloaded from the website (<http://paleoecologie.umontreal.ca/public/code/SEA.m>). The period analysed (time window) is set as 20 years before and after each volcanic eruption event. The 90 % confidence limit is estimated using the bootstrap procedure (Blarquez and Carcaillet, 2010). The eruption time series of Sigl et al. (2015) is used here because of the dating improvement compared to earlier estimates. Four categories of volcanic eruption events during the period from AD 1490 to AD 1829 are chosen fol-

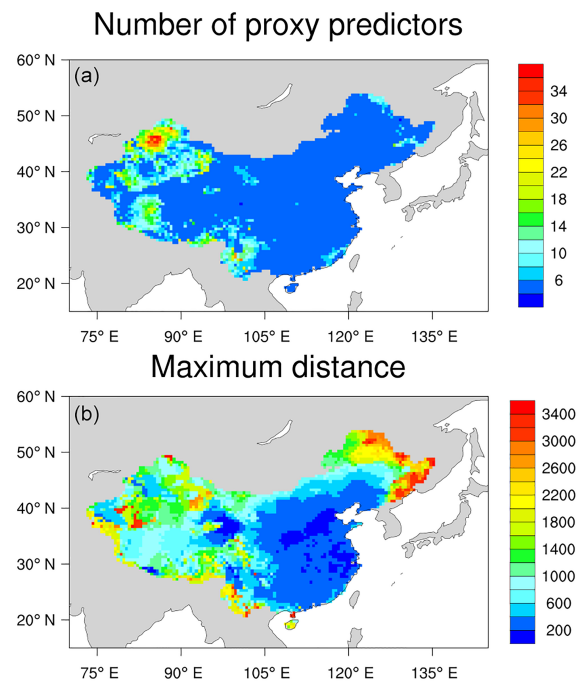


Figure 2. The spatial distributions of the number of proxy predictors (a) and the maximum distance from the predictor to the target (b) for each grid point.

lowing Zhuo et al. (2014)'s method, which is based on the magnitude of their sulfate deposition in the Greenland ice-core records: (1) all Northern Hemisphere eruption events (CNH0P) according to Sigl et al. (2015), (2) CNH1/2P: the eruption events that have more than half, (3) equal (CNH1P), and (4) double (CNH2P) the sulfate deposition of the 1991 Mount Pinatubo eruption.

3 Results and discussion

The quality and reliability of the reconstruction are illustrated in Figs. 2–4. Firstly, the spatial distribution of the number of predictors for each grid is shown in Fig. 2a. As mentioned above, the initial minimum number of predictors is five. 2599 grid points with five candidate proxy records account for 62.04 % of the total number of grid points. 3760 grid points with ≤ 10 candidate proxy records account for 89.76 %. The maximum number of predictors is 38. Only seven grids cannot satisfy the initial minimum number of predictors (five). This indicates that 99.86 % grids have good replication of the reconstruction. In order to reconstruct these seven grids, we tolerate the four grids with four predictors, and the three grids with three predictors. This means that these seven grids did not followed the requirement of the replication. Secondly, the maximum distance from the predictor to the target for each grid is shown in Fig. 2b. 1599 grid points have a search radius ≤ 450 km, accounting for 38.17 % of the total number of points. 3467 grid points with search radii ≤ 1500 km ac-

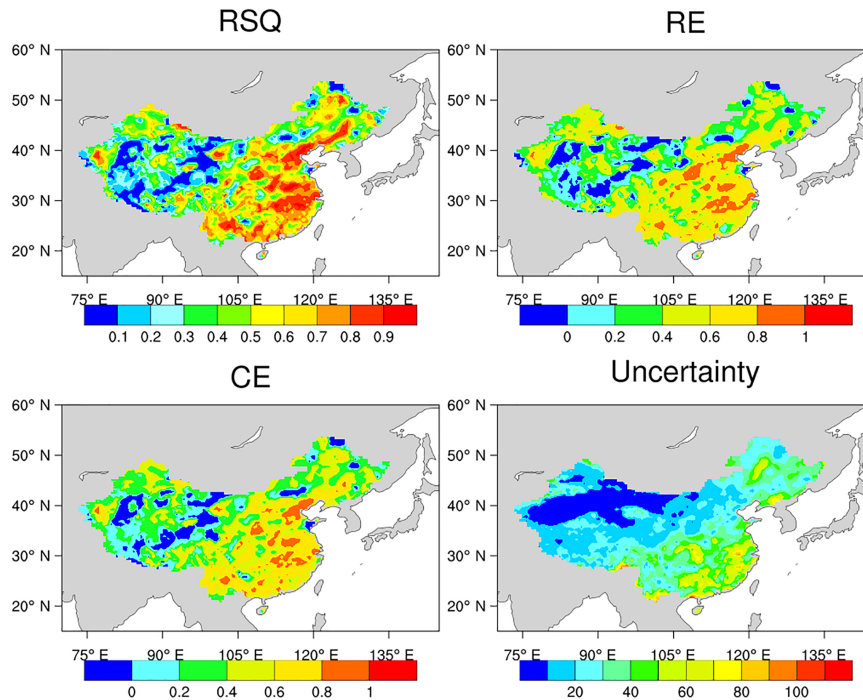


Figure 3. Skills of the reconstructed MJJAS mean precipitation anomalies in China for the 1961–1990/1991–2000 calibration/verification period. The r^2 is the square of the Pearson product–moment correlation coefficient, the RE and CE are the reduction of error and the coefficient of efficiency, and the uncertainty is characterized by the standard deviation of the residual between the reconstructed and instrumental precipitation data during the verification period.

count for 82.76%. The maximum distance to the target is 3495.5 km. This implies that precipitation in most of the grid points can be reconstructed using nearby proxy records.

Thirdly, Fig. 3 presents a summary of the reconstruction skills. Figure 3a–c show that the similarity in the patterns among the r^2 , the RE, and the CE maps, characterized by a better quality of the reconstruction in eastern China (with the exception of some regions in northeastern China) than in western China. The maximum explained variance is 0.96. The number of grid points for which both the RE and CE values are greater than zero is 3631, accounting for 86.68% of the grids. This indicates that most of the grid points pass the cross-validation process. The absolute uncertainties associated with the grid points in southeastern China are greater than those for the grid points in northwestern China in Fig. 3d because of large precipitation anomalies in southeastern China.

Finally, Fig. 4 shows a good agreement between the reconstructed MJJAS mean precipitation anomalies and the instrumental MJJAS mean precipitation anomalies (Zhao and Zhu, 2015) for China for the interval AD 1961–2000. The correlation coefficient between the two time series is 0.89 ($n = 40$), which is significant at the 99% confidence level. Figure 4 also compares the reconstructed MJJAS mean precipitation anomalies with the instrumental MJJAS mean precipitation anomalies (Li et al., 2012) in China during AD 1900–2000.

The reconstructed MJJAS mean precipitation anomaly is significantly correlated to the instrumental independent data during the interval AD 1920–1960, with a correlation coefficient of 0.59 ($n = 41$), also significant at the 99% confidence level. This indicates that the reconstruction passes the out-of-sample validation on the mean MJJAS precipitation anomalies for China. A part of the disagreements before AD 1919 can come actually from the uncertainties of Li et al. (2012), as explained in Sect. 2.

The evolution of regional mean precipitation anomalies is exhibited in Fig. 5. The different components of the MJJAS precipitation anomalies for eastern China (east of 105° E), western China (west of 105° E), and the whole of China over the past 531 years (AD 1470–2000) are obtained using the EEMD method (Figs. 5 and S4). The amplitudes of interannual and interdecadal components in eastern China are much larger than in western China (Fig. S4), but the differences of the amplitudes of other components between eastern and western China are less clear in Fig. 5. The drought/flood changes in eastern and western China are generally consistent over the multidecadal timescale in Fig. 5a.

The centennial components in eastern and western China describe both a relatively wet climate during the 16th century and a drought during the 17th century. The 17th-century drought is also reported in previous studies (e.g. Wang et al., 2002). The correlation coefficient of the centennial com-

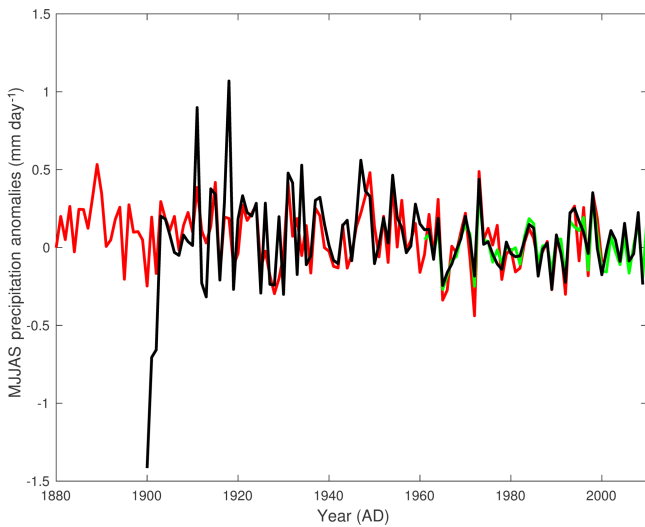


Figure 4. Comparison of the reconstructed (red line) and instrumental MJJAS mean precipitation anomalies for China. The correlation coefficients are $r = 0.89$ ($n = 40$, AD 1961–2000) for instrumental data (green line; Zhao et al., 2015), and $r = 0.59$ ($n = 41$, AD 1920–1960) for instrumental data (black line; Li et al., 2012).

ponent in eastern and western China during the interval AD 1470–1749 is 0.87, but the correlation coefficient during the interval AD 1750–2000 is -0.62 . Moreover, the 101-year running correlation between the centennial components in eastern and western China shows that a strongly significant positive relationship gradually changed to a weakly significant negative relationship during the late 18th century (figure not shown). This may suggest that the driver of the centennial component changed after the late 18th century.

The long-term trends in eastern and western China have opposite signs. The long-term trend in eastern China can be broadly divided into two periods: during the first phase before the early 18th century there was a wetting trend, and then the conditions become dryer until now. This is consistent with previous studies (e.g. Zheng et al., 2006; Pei et al., 2015). The long-term trend in western China can also be divided two stages: during the first stage from the late 15th century to the late 16th century there was a drying trend; the second stage corresponds to gradually wetter conditions until now. The long-term trend for the whole of China has similarities with that in eastern China, but with a much weaker amplitude.

Figure 6 shows the spatial patterns of the May–September precipitation field relative to the 1961–1990 climatological mean during five severe droughts in China. The selection of five drought periods follows Feng et al. (2013) but the spatial patterns in our reconstruction display some clear differences from their results. A “north drought with south flooding” dipole pattern in eastern China is seen in Fig. 6a–d, and there is a three-pole pattern in eastern China in Fig. 6e. A similar dipole pattern can be found in Fig. 5b and d of

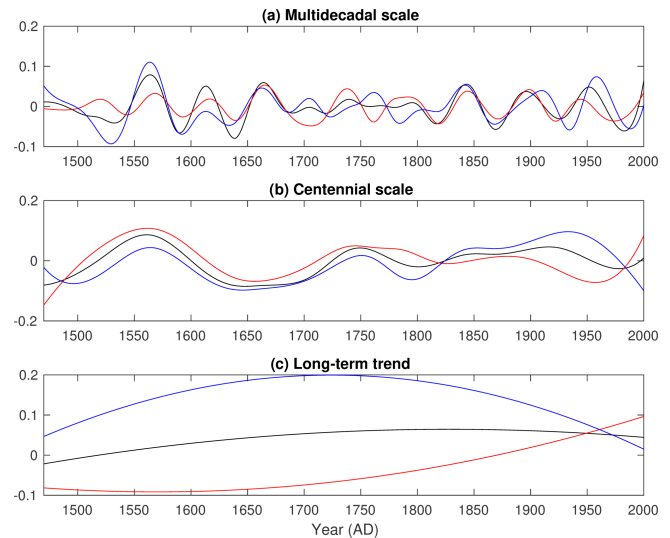


Figure 5. The intrinsic mode functions (IMFs) of the mean MJJAS precipitation anomalies for eastern China (blue line), western China (red line), and the whole of China (black line), over the past 531 years (AD 1470–2000) using the ensemble empirical mode decomposition (EEMD) method, including the multidecadal component (a), centennial component (b), and long-term trend (c).

Feng et al. (2013) for two drought events (AD 1586–1589 and AD 1876–1878) but during four out of five drought periods, most of northeastern China is relatively humid in our study, which is not consistent with Feng et al. (2013)’s Fig. 5. An exceptional drought condition in northeastern China appears in the 1876–1878 drought event, which is the most severe drought of five events in eastern China.

We have also calculated the spatial correlation between Cook’s MADA PDSI reconstruction (Cook et al., 2010) and our precipitation reconstruction in Fig. S3. Strong correlations are obtained in the northeastern Tibetan Plateau, where there are the longest and most abundant tree-ring width chronologies in China. Here, the precipitation is possibly a primary control factor of the tree-ring width chronology (Q. Zhang et al., 2003; Yang et al., 2014b). There are weak correlations between the reconstructions in eastern China even though the correlation coefficients are significant in some regions. The MADA is not consistent with the DWI records in eastern China, since only very few and short tree-ring width chronologies in eastern China are used to reconstruct the MADA (Yang et al., 2013a, 2014a; Kang et al., 2014; Zheng et al., 2014b; Ge et al., 2016).

We compared the precipitation reconstruction with the six climate model simulations in Figs. 7–8. The analysis period is from AD 1470. Before that date, there are no available historical documents and the quality of the reconstruction is thus likely low. The analysis of spatial patterns covers the period AD 1470–1849 as we specifically focus on the pre-industrial period. The more recent past has been the subject of some recent studies, and different factors such as the

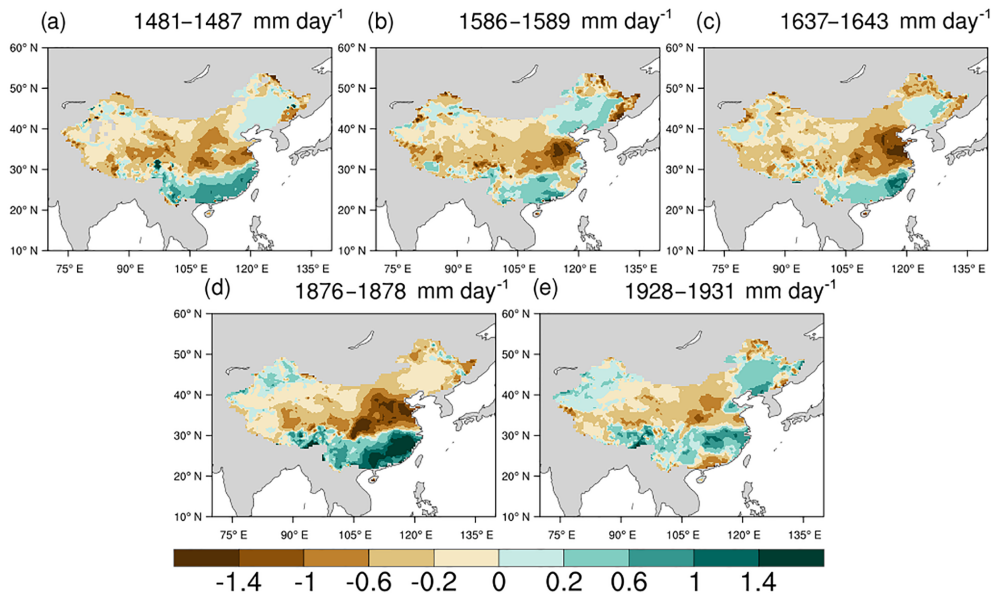


Figure 6. Spatial patterns of the May–September precipitation field relative to the 1961–1990 climatological mean during five severe droughts in China.

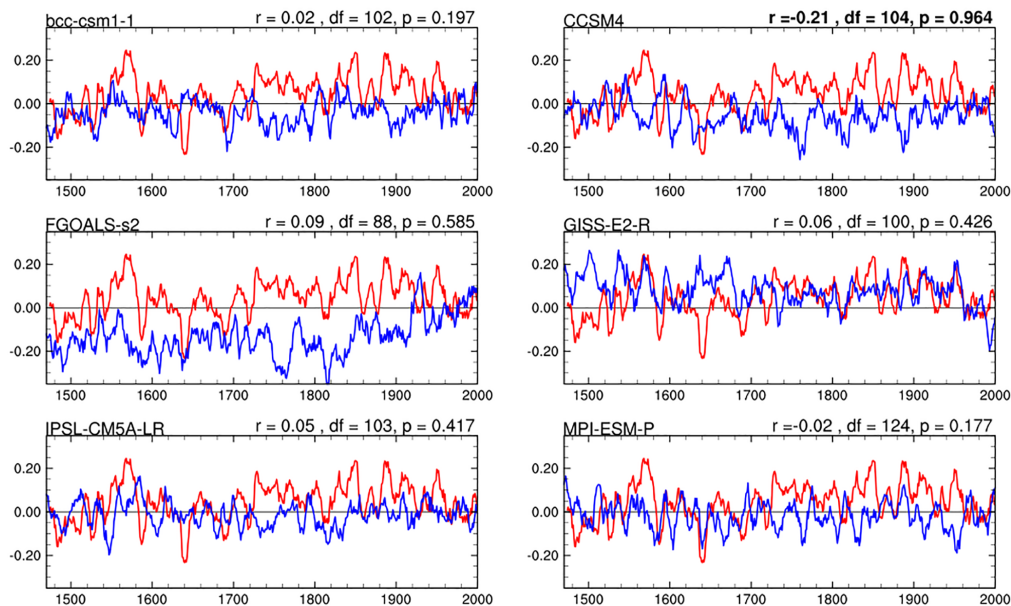


Figure 7. Comparison of the reconstructed 9-year running mean (red line) and six simulated (blue line) MJJAS mean precipitation anomalies for China during the interval AD 1470–2000.

changes in aerosol concentration may have a dominant effect (Li et al., 2016). Figure 7 shows the reconstructed 9-year running mean MJJAS precipitation anomalies for China for the interval AD 1470–2000 compared with six climate model simulations. Only the CCSM4 results are significantly correlated with the reconstructed results during the interval AD 1470–1849 at the 95 % confidence level, but the correlation is low and negative ($r = -0.16$). Furthermore, there is

a distinct shift between the mean values of the CCSM4 results and the reconstruction over that period. This is related to the choice of the reference period. All climate model simulations show low correlations with the reconstructed result. The correlation of the simulated time series is also weak between the different models. This suggests that MJJAS mean precipitation anomalies over the past 380 years in China may be largely controlled by the internal variability rather than by

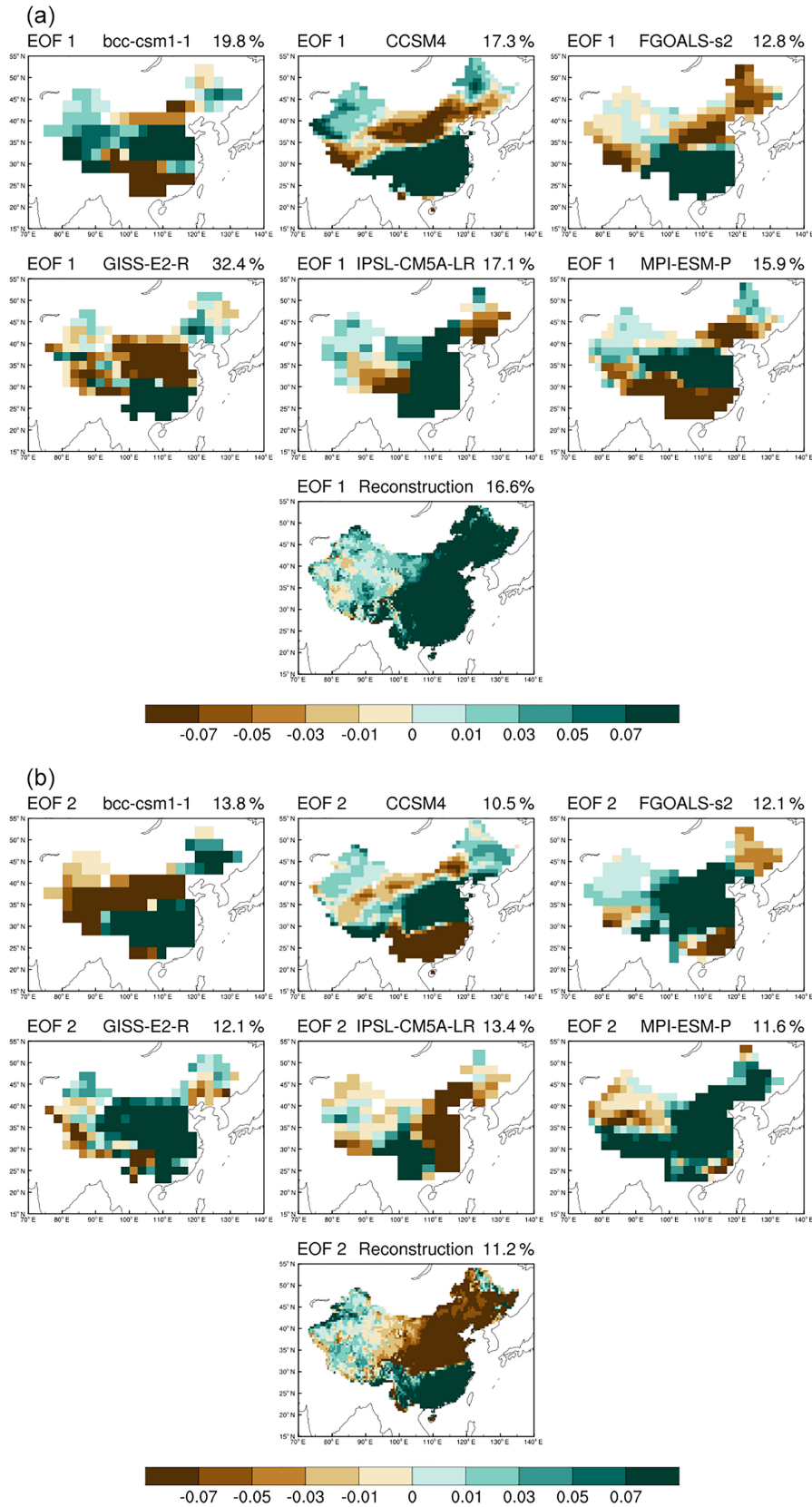


Figure 8.

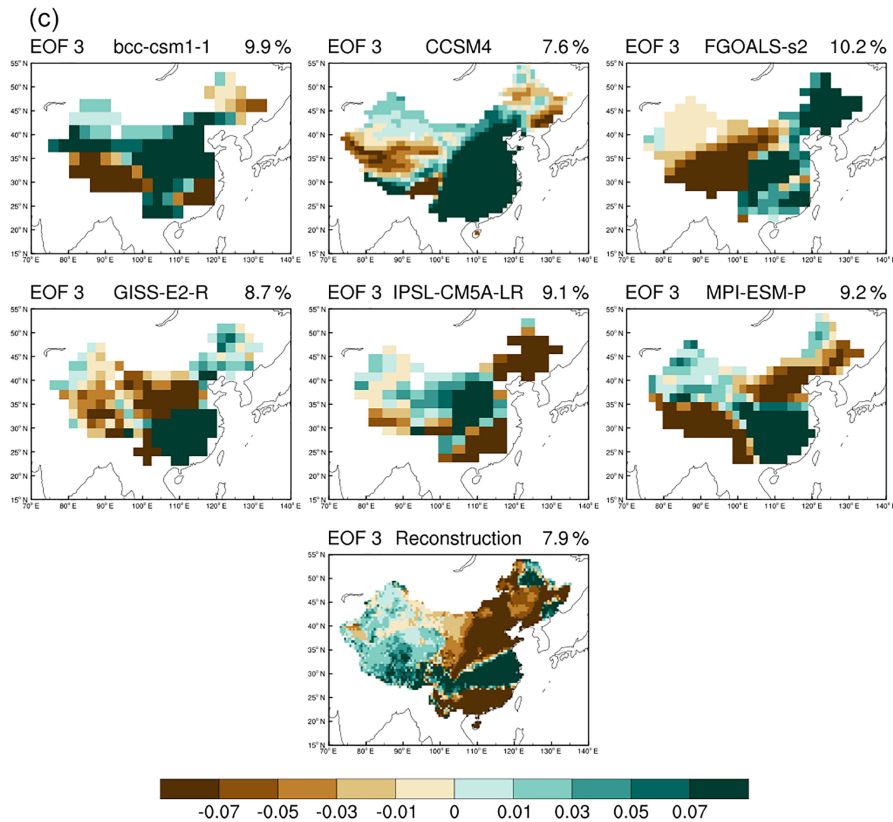


Figure 8. (a) Empirical orthogonal function (EOF) 1 of the MJJAS mean precipitation anomalies for China during the interval AD 1470–1849. (b) Empirical orthogonal function (EOF) 2 of the MJJAS mean precipitation anomalies for China during the interval AD 1470–1849. (c) Empirical orthogonal function (EOF) 3 of the MJJAS mean precipitation anomalies for China during the interval AD 1470–1849.

external forcing during the interval (AD 1470–1849). Similar conclusions were derived from the comparison of reconstructed and simulated hydroclimatic variables over the past millennium in North America (Coats et al., 2015) and in East Africa (Klein et al., 2016).

Traditional EOF analysis was applied to reveal the spatial patterns in MJJAS precipitation anomalies in China over a 380-year interval (AD 1470–1849). The first four EOFs are well separated according to North et al. (1982) criteria, but the fourth EOF only accounts for 4.7 % of total variance, and its pattern is unusual compared to previous studies. Thus, the first three EOF patterns and their corresponding time coefficients (also known as principal components, PCs) of the reconstructed MJJAS precipitation fields in China are compared with six climate model simulations in Fig. 8.

The first EOF leading mode of the reconstructed MJJAS precipitation field (Fig. 8a) displays a main loading in eastern China, and a general (monopole) variation over most of China, with the exception of the northeastern and western margins of the Tibetan Plateau. The explained variance in this mode accounts for 16.6 % of the total variance, and lower than that in the leading mode of temperature field (Shi et al., 2015a), but this is normal in precipitation anal-

ysis (Day et al., 2015). A main loading in eastern China also appears in the EOF1 of the reconstructed MJJAS precipitation anomalies during the interval AD 1850–2000, the EOF1 of the reconstructed data during the interval AD 1961–2000, and the EOF1 of the instrumental data during the same interval (AD 1961–2000). A main loading of EOF1 in eastern China is also consistent with other previous results (Wang and Zhao, 1979; Qian et al., 2003a). This is due to the large variance in eastern China, which also causes the larger loads in eastern China in the other two EOFs. The EOF1 of IPSL-CM5A-LR, the EOF2 of MPI-ESM-P, and the EOF3 of CCSM4 also show a consistent variation in most of eastern China, but also some differences with the pattern deduced from the reconstruction. Furthermore, the corresponding time coefficients of model EOFs show no obvious significant relationship with the reconstructed data (figure not shown), which would be expected if natural variability is the main driver of the changes.

The second leading mode of the MJJAS precipitation field (Fig. 8b) demonstrates a south–north anomalous rainfall dipole pattern, with drying in the middle and lower reaches of the Yellow River, and increasing rainfall to the south of the Yangtze River. This mode accounts for 11.2 % of the

total variance and also appears in the EOF2 of the reconstructed MJAS precipitation anomalies during the interval (AD 1850–2000). The south-flood north-drought pattern is commonly referred to in previous studies from an analysis of DWI (e.g. Wang and Zhao, 1979; Qian et al., 2003a) and instrumental data (e.g. Huang et al., 1999; Yu and Zhou, 2007; Ding et al., 2008; Zhou et al., 2009). Moreover, the variations have the same sign in most of western China and northern China, except for Xinjiang province. The EOF1 from three climate models (CCSM4, FGOALS-s2, GISS-E2-R), the EOF2 from BCC-CSM1.1 model, and the EOF3 from MPI-ESM-P model reproduce a south–north dipole pattern in eastern China similar to the reconstructed results, but the specific range for each model is different. Moreover, their corresponding time coefficients show that no climate model simulation demonstrates a significant relationship with the reconstructed result (figure not shown). As mentioned for EOF1, this may be perfectly well justified if the variability of the south–north dipole pattern is dominated by internal variability.

The third leading mode illustrates a “sandwich” three-pole precipitation pattern with increasing rainfall in the area covering the middle and lower reaches of the Yangtze River valley, drying over southern and northern China, and variations of the same sign in most of western China and central China (Fig. 8c). This mode accounts for 7.9 % of the total variance. The “sandwich” three-pole mode in eastern China has been reported based on the analysis of DWI (e.g. Wang and Zhao, 1979; Qian et al., 2003b) and instrumental data (e.g. Ding et al., 2008). The EOF1 from two climate models (BCC-CSM1.1 and MPI-ESM-P), the EOF2 from CCSM4 model, and the EOF3 from IPSL-CM5A-LR model show similar “sandwich” three-pole mode to the reconstruction, and their corresponding time coefficients have again no significant relationship with the reconstructed result at the 90 % confidence level (figure not shown).

In order to explore the origins of three dominant modes, we firstly consider the influence of the external forcing on the MJAS precipitation anomalies variability during the interval AD 1470–1849. The impact of the Northern Hemisphere volcanic eruptions on the precipitation field for the four categories of eruption (CNH0P, CNH1/2P, CNH1P, and CNH2P) is shown in Fig. S5. The superposed epoch analysis results applied to the mean precipitation anomalies (Fig. S5a), and its PC1 (Fig. S5b) during the interval AD 1490–1829 shows that volcanic activity as one important external forcing might affect the MJAS precipitation anomalies variability for China. Nevertheless, the signals are barely significant and there are similar averaged scores before and after the volcanic eruption year. Moreover, the spatial pattern of the impact of the Northern Hemisphere volcanic eruption events on the precipitation field (Fig. S5c–f) is not consistent among the four categories of eruption (CNH0P, CNH1/2P, CNH1P, and CNH2P). This indicates that the response of MJAS pre-

cipitation anomalies for China to northern hemispheric volcanic eruption is not robust.

The solar activity, as another potentially important external forcing, may also be part of the driving mechanism. This view is supported by the fact that the PC1 shows a weak significant relationship with solar activity index (Wang et al., 2005) ($r = 0.19$, $n = 240$) at the 95 % confidence level for the interval AD 1610–1849. The correlation coefficient reaches 0.35 after applying an 11-year running mean filter. In summary, the influences of volcanic eruption and solar activity on PC1 are not very strong in our results.

A pattern showing some similarities to the PC1 of the reconstructions appears in three climate models (Fig. 8a), but the differences, in particular in western China, are too large to ensure that it has the same dynamical origin and therefore to use model results to determine the origin of the reconstructed pattern. The second mode of annual precipitation field is the north–south dipole mode in eastern China, with variations of the same sign in most of western China and northern China, except for Xinjiang province. In fact, the north–south dipole pattern of the precipitation in eastern China was found over the centennial timescale during the Medieval Warm Period and the Little Ice Age from the historical documents and speleothem records (e.g. Wang et al., 2001) and was one of the dominant modes over the interdecadal timescale (e.g. Ding et al., 2008).

In order to explore its possible origin, we have calculated the running correlation between the 17 reconstructed ENSO indices and the precipitation anomalies averaged over the Yangtze River region and Huai River region with a window size of 101 years (figures not shown). The correlation varied between negative and positive values, and a small but positive correlation is obtained for the full period. This indicates that the relationship between ENSO and summer precipitation in China is not stable in time, which is consistent with the instrumental period (Wu and Wang, 2002). However, if we analyse the full period, a more robust link between ENSO and summer precipitation in China may be found on average.

We calculated the correlation of the precipitation field with the annual mean (over the months July–June) ENSO index of McGregor et al. (2010), as shown in Fig. 9. The results show a similar pattern with a north–south dipole mode in eastern China, and the precipitation anomalies in most of western China have a positive correlation with ENSO at the 90 % confidence level. In addition, PC2 is significantly correlated with the ENSO index reconstruction (McGregor et al., 2010) at the 99 % level ($r = 0.30$, $n = 200$) during the interval AD 1650–1849. Moreover, two other ENSO indices (Cook et al., 2008; Li et al., 2013a) give similar correlation maps with the precipitation field (Fig. S6), but lower correlation coefficients with PC2. This indicates that the north–south dipole in eastern China and variations of the same sign in most of western China and northern China, except for Xinjiang province, are likely influenced by ENSO variability before the Industrial Revolution in our reconstruction.

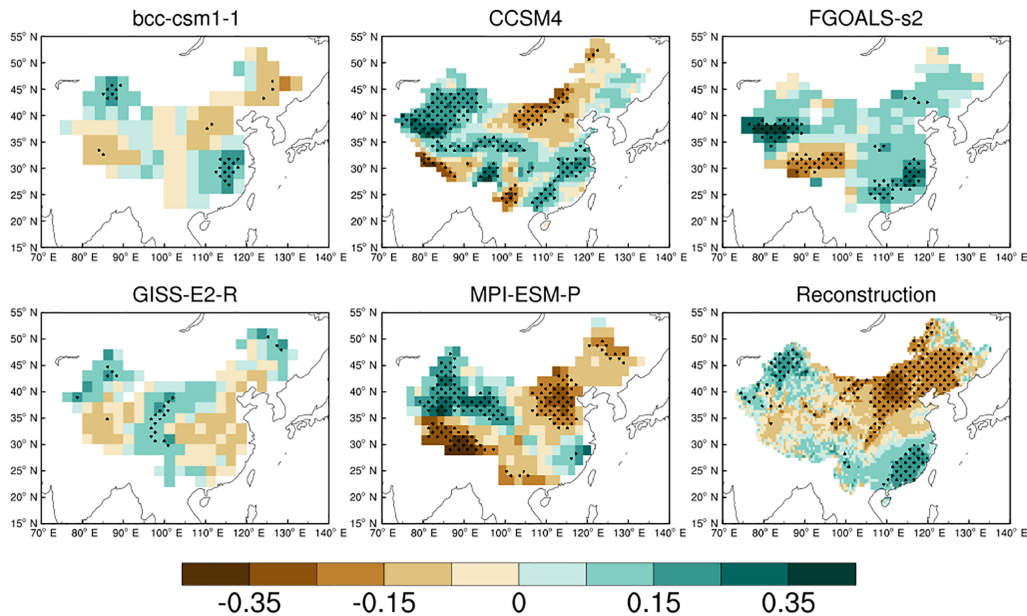


Figure 9. Correlation maps of five simulated and reconstructed MJJAS mean precipitation anomalies for China with the five corresponding simulated annual mean Niño 3.4 indices and a reconstructed annual mean ENSO index (McGregor et al., 2010).

Finally, we calculated the simulated Niño 3.4 in different seasons including the annual mean (over the months July–June), previous July to current June, previous December–January–February (DJF), current March–April–May (MAM), current June–July–August (JJA), and current MJJAS seasons. The correlation maps of five simulated MJJAS mean precipitation anomalies for China with the five corresponding simulated annual mean Niño 3.4 indices are shown in Fig. 9. They display similar south–north dipole correlation patterns in eastern China (similar to the one from the reconstruction) for three climate models (BCC-CSM1-1, CCSM4, and MPI-ESM-P). The relationship between the previous winter (December–January–February) Niño 3.4 index and the precipitation field for each model is shown in Fig. S7. The spatial pattern is very similar with the result of annual mean Niño 3.4 index. The Niño 3.4 indices in previous July to current June, previous December–January–February (DJF), and current March–April–May (MAM) seasons during AD 1470–1849 in CCSM4 model are significantly related to its PC1 at the 99 % confidence level, and the correlation coefficients are 0.30, 0.30, and 0.27, respectively. The Niño 3.4 indices in current June–July–August (JJA) and MJJAS seasons in FGOALS-s2 model during AD 1470–1849 are significantly related to its PC1 at the 99 % confidence level, and the correlation coefficients are both 0.16. The Niño 3.4 indices in previous July to current June, previous DJF, current MAM, JJA, and MJJAS seasons during AD 1470–1849 in MPI-ESM-P model are significantly related to its PC3 at the 99 % confidence level, and the correlation coefficients are 0.23, 0.22, 0.20, 0.18, and 0.19, respectively. The EOF1 of CCSM4 model, the EOF1 of FGOALS-

s2 model, and the EOF3 of MPI-ESM-P model all show a similar south–north dipole mode, even though the specific ranges of their spatial patterns are different. This demonstrates that ENSO has likely an imprint on the south–north dipole mode of the precipitation pattern in eastern China during the interval AD 1470–1849 in those simulations.

These results are consistent with previous studies based on PMIP3 model simulations suggesting that La Niña (El Niño)-like conditions may explain the north–south dipole in eastern China on the centennial timescale (e.g. Shi et al., 2016) and with instrumental observations indicating that ENSO was associated with summer rainfall in eastern China (e.g. Huang and Wu, 1989; Guo et al., 2012; Schubert et al., 2016). Based on instrumental data analysis, three hypotheses have been proposed to explain the link between the precipitation variability in eastern Asia and ENSO. All of them emphasize the important role of the anomalous western North Pacific anticyclone. The first one mentions the equatorial Rossby wave response to ENSO via the Pacific–East Asia teleconnection (Wang et al., 2000; Zhang et al., 2011; Karori et al., 2013; Feng et al., 2016). The second one is related to an equatorial Kelvin wave response to Indian Ocean warming during El Niño decaying summer, which is named “Indian Ocean capacitor effect” (Xie et al., 2009). The third one is more recent and is based on the nonlinear atmospheric interactions between ENSO and the annual cycle (Stuecker et al., 2013; Zhang et al., 2016).

We calculated the correlation map of the precipitation field with the PDO index (D’Arrigo et al., 2001) applying a 9-year running mean filter (Fig. S2). The results at the 90 % confidence level show a pattern similar to EOF2 with a north–

south dipole mode in eastern China. Moreover, the relationship between PDO index (D'Arrigo et al., 2001) and PC2 is strongly significant ($r = 0.41$, $n = 150$) during the interval AD 1700–1849 at 95 % confidence level after a 9-year running mean filter. However, the other two PDO indices (D'Arrigo and Wilson, 2006; Shen et al., 2006) give different correlation maps with the precipitation field (Fig. S2), and lower correlation coefficients (-0.25 and 0.36) with PC2 after a 9-year running mean filter. This indicates that the EOF2 mode is also possibly related to variations in the PDO, but the result is sensitive to the choice of the reconstructed PDO index.

Based on the instrumental data analysis, the “sandwich” three-pole mode in eastern China is likely associated with a meridional teleconnection in eastern Asia linked to the Pacific–Japan (PJ; Nitta, 1987), the Pacific–East Asia (EAP, Huang and Li, 1988), or Indo–Asia–Pacific (IAP; Li et al., 2013b). The PJ/EAP/IAP teleconnection pattern can be considered as an internal mode mainly controlled by atmospheric processes (Hirota and Takahashi, 2012; Zhang and Zhou, 2015). It can also be forced by external heating such as the anomalous convective activity in the western Pacific and tropical Indian Ocean during the El Niño decaying year (Huang and Li, 1988; Li et al., 2013b; Xie et al., 2009; B. Wu et al., 2010). However, there is no direct evidence from the correlation maps of the reconstructed precipitation field with the ENSO and PDO indices to support this kind of mechanism for the “sandwich” pattern in this study. Alternatively, a new hypothesis was proposed recently to explain the “sandwich” three-pole mode through the interannual change in the strength of moisture transport from the Bay of Bengal to the Yangtze corridor across the northern Yunnan Plateau (Day et al., 2015). An increased latent heating associated with an increase in water vapour along the Yangtze corridor may generate variations of the same sign in most of western China and central China as in the three-pole mode in eastern China obtained in our EOF analysis.

Our results indicate thus that the south–north mode variability of precipitation anomalies in China carries very likely the fingerprint of ENSO evolution in the tropical Pacific over the past 500 years. The origin of the EOF1 and EOF3 patterns over the pre-industrial period is not clearly established yet, even though both of them may be related to the movement and intensity of the western Pacific subtropical high during the instrumental period (Wu and Wang, 2002). Moreover, some studies show that other factors such as the North Atlantic Oscillation (NAO) (Wu et al., 2009; Zheng et al., 2016) and the North Atlantic three-pole SST pattern (Ruan and Li, 2016), the interdecadal Pacific oscillation (IPO) (Song and Zhou, 2015), the snow cover change of the Tibetan Plateau (Ding et al., 2009; Wu et al., 2012), and some regional processes in China may contribute to the precipitation field modes during the instrumental period. Thus, additional studies are required to determine which of these processes might be related to EOF1 and EOF3 over the pre-industrial period.

Some climate models (e.g. CCSM4, MPI-ESM-P) can broadly reproduce some of the dominant spatial patterns of variability of the reconstructed precipitation field for the period studied. Nevertheless, the corresponding time coefficients do not match with the reconstructed series. A possible reason for this is that the precipitation changes are controlled by internal variability (e.g. related to ENSO). By constraining model result to follow the observed time series, data assimilation may then provide an interesting opportunity to analyse more detailed mechanisms at the origin of the reconstructed changes (e.g. Widmann et al., 2010; Hakim et al., 2016).

4 Conclusions

The precipitation field for the whole of China was reconstructed for the past half millennium using the OIE method and additional proxy records compared to previous studies. The reconstruction shows good performance through the cross-validation process and through comparison with “out-of-sample” instrumental data.

The precipitation field reconstruction reveals three leading modes for the period AD 1470–1849 before the Industrial Revolution. The first dominant mode shows consistent variation across most of China, with the exception of the northwestern Tibetan Plateau and some areas of the Xinjiang province. This mode does not appear to be associated with the response to volcanic eruption or solar activity. A hypothesis is that such homogeneous precipitation variations in various climate regions in China have their origin in the internal variability of the system, but it was not possible to determine in the present framework through which mechanism. The second mode comprised a north–south dipole in eastern China and variations of the same sign in most of western China and northern China, except for Xinjiang province. The correlation with different reconstructions of ENSO index indicates that this dipole is likely related to variations in ENSO. The third mode is a “sandwich” three-pole mode in eastern China and variations of the same sign in most of western China and central China.

Moreover, the precipitation field reconstruction was used to assess the skill of PMIP3 coupled climate models. For most models, the dominant mode of variability is not characterized by relatively homogeneous changes over all China, in contrast to the reconstructed fields. The correlation maps between the five simulated MJJAS mean precipitation anomalies for China and the five corresponding simulated annual mean Niño 3.4 indices show that the ENSO has likely an imprint on the south–north dipole mode of precipitation anomaly in eastern China over the half past millennium in the simulations too. However, there is a model–reconstruction mismatch in reproducing the corresponding time development, as the models are not able to reproduce the timing of events associated with internal variability.

Data availability. The 479 proxy records include 361 tree-ring width chronologies and a tree-ring $\delta^{18}\text{O}$ chronology archived in International Tree Ring Data Bank (ITRDB) (<https://www.ncdc.noaa.gov/data-access/paleoclimatology-data/datasets/tree-ring>), 10 tree-ring width chronologies, and 107 Dryness/wetness records at the web pages of the Chinese Meteorological Data Service Center (CMDC) (http://data.cma.cn/data/detail/dataCode/HPXY_TRRI_CHN.html, and http://data.cma.cn/data/detail/dataCode/HPXY_HDOC_CHN_DAW.html). A link (URL) for the original record is included in Table S1 in the Supplement, which is to the location where the original record is stored in the public repository. The two instrumental precipitation datasets are both archived by the CMDC. The China Ground Precipitation Dataset V2.0 can be obtained from the website (http://data.cma.cn/data/detail/dataCode/SURF_CLI_CHN_PRE_MON_GRID_0.5.html) and the Homogenized Monthly Precipitation Dataset in China can be downloaded from the website (http://data.cma.cn/data/detail/dataCode/SEVP_CLI_CHN_PRE_MON_GRID.html). Registration is required to obtain these records from the web of CMDC. We have archived the detrended and infilled version of 362 tree-ring chronologies to NOAA website (<https://www.ncdc.noaa.gov/paleo/study/23056>). The other 10 tree-ring width chronologies have already been detrended, and from the website of CMDC. The script of the regularized expectation maximization (RegEM) method is available at <http://climate-dynamics.org/software/#regem> and can be easily used to extend these chronologies to AD 2000. Moreover, we have archived the code for the OIE (version 1.3) method and the precipitation reconstruction (IGGPRES.1.0.anom.nc) to NOAA website (<https://www.ncdc.noaa.gov/paleo/study/23056>).

The Supplement related to this article is available online at <https://doi.org/10.5194/cp-13-1919-2017-supplement>.

Competing interests. The authors declare that they have no conflict of interest.

Special issue statement. This article is part of the special issue “Climate of the past 2000 years: regional and trans-regional syntheses”. It does not belong to a conference.

Acknowledgements. This work was jointly funded by the National Key R&D Program of China, Ministry of Science and Technology of the People’s Republic of China (Grant No. 2016YFA0600504), and the National Natural Science Foundation of China (Grants No. 41505081, No. 41690114, and No. 41430531). Feng Shi was supported by the “MOVE-IN Louvain” Incoming Post-doctoral Fellowship, co-funded by the Marie Curie actions of the European Commission. Hugues Goosse is Research Director and Qiuzhen Yin is Research Associate with the FNRS-Fonds de la Recherche Scientifique, Belgium. We thank François Klein for his help in the processing of the data. Thanks are extended to Kevin J. Anchukaitis, Hemant P. Borkanar, Achim Bräuning, Brendan M. Buckley, Edward R. Cook,

Zexin Fan, Keyan Fang, Narayan P. Gaire, Xiaohua Gou, Minhui He, Katsuhiko Kimura, Paul J. Krusic, Jiangfeng Li, Jinbao Li, Hongbing Liu, Chun Qin, Jonathan G. Palmer, Tatyana Papina, Jianfeng Peng, Somaru Ram, Masaki Sano, Margit Schwikowski, Xuemei Shao, Paul Sheppard, Jiangfeng Shi, Shri A. B. Sikder, Olga Solomina, Jianglin Wang, Bao Yang, Koh Yasue, Yujia Yuan, Xiyao You, Muhammad Usama Zafar, Masumi Zaiki, Wensheng Zhou, and other paleoclimatic scientists who published the various tree-ring chronologies used in this study.

Edited by: Hans Linderholm

Reviewed by: three anonymous referees

References

- Blarquez, O. and Carcaillet, C.: Fire, fuel composition and resilience threshold in subalpine ecosystem, *PLoS One*, 5, e12480, <https://doi.org/10.1371/journal.pone.0012480>, 2010.
- Bradley, R. S.: The explosive volcanic eruption signal in Northern Hemisphere continental temperature records, *Climatic Change*, 12, 221–243, <https://doi.org/10.1007/BF00139431>, 1988.
- Casty, C., Wanner, H., Luterbacher, J., Esper, J., and Böhm, R.: Temperature and precipitation variability in the European Alps since 1500, *Int. J. Climatol.*, 25, 1855–1880, <https://doi.org/10.1002/joc.1216>, 2005.
- Chinese Academy of Meteorological Science: China Meteorological Administration (CMA), Yearly charts of dryness/wetness in China for the last 500-year period, Cartological Press, Beijing, China, 1981 (in Chinese).
- Christiansen, B.: Reconstructing the NH mean temperature: Can underestimation of trends and variability be avoided?, *J. Climate*, 24, 674–692, <https://doi.org/10.1175/2010jcli3646.1>, 2011.
- Christiansen, B. and Ljungqvist, F. C.: Reconstruction of the extratropical NH Mean temperature over the last millennium with a method that preserves low-frequency variability, *J. Climate*, 24, 6013–6034, <https://doi.org/10.1175/2011jcli4145.1>, 2011.
- Christiansen, B. and Ljungqvist, F. C.: Challenges and perspectives for large-scale temperature reconstructions of the past two millennia, *Rev. Geophys.*, 55, 40–96, <https://doi.org/10.1002/2016RG000521>, 2017.
- Coats, S., Smerdon, J. E., Cook, B. I., and Seager, R.: Are simulated megadroughts in the North American southwest forced?, *J. Climate*, 28, 124–142, <https://doi.org/10.1175/JCLI-D-14-00071.1>, 2015.
- Cook, B. I., Ault, T. R., and Smerdon, J. E.: Unprecedented 21st century drought risk in the American Southwest and Central Plains, *Sci. Adv.*, 1, e1400082, <https://doi.org/10.1126/sciadv.1400082>, 2015.
- Cook, E. R., Meko, D. M., Stahle, D. W., and Cleaveland, M. K.: Drought reconstructions for the continental United States, *J. Climate*, 12, 1145–1162, [https://doi.org/10.1175/1520-0442\(1999\)012<1145:DRFTCU>2.0.CO;2](https://doi.org/10.1175/1520-0442(1999)012<1145:DRFTCU>2.0.CO;2), 1999.
- Cook, E. R., Woodhouse, C. A., Eakin, C. M., Meko, D. M., and Stahle, D. W.: Long-term aridity changes in the western United States, *Science*, 306, 1015–1018, <https://doi.org/10.1126/science.1102586>, 2004.
- Cook, E. R., D’Arrigo, R. D., Anchukaitis, K. J., and Diaz, H. F.: 700 Year Tree-Ring ENSO Index Reconstructions, available

- at: <https://www.ncdc.noaa.gov/paleo/study/8704> (last access: 19 December 2017), 2008.
- Cook, E. R., Anchukaitis, K. J., Buckley, B. M., D'Arrigo, R. D., Jacoby, G. C., and Wright, W. E.: Asian monsoon failure and megadrought during the last millennium, *Science*, 328, 486–489, <https://doi.org/10.1126/science.1185188>, 2010.
- Cook, E. R., Krusic, P. J., Anchukaitis, K. J., Buckley, B. M., Nakatsuka, T., Sano, M., and PAGES Asia2k Members: Tree-ring reconstructed summer temperature anomalies for temperate East Asia since 800 CE, *Clim. Dynam.*, 41, 2957–2972, <https://doi.org/10.1007/s00382-012-1611-x>, 2013.
- Cook, E. R., Seager, R., Kushnir, Y., Briffa, K. R., Büntgen, U., Frank, D., Krusic, P. J., Tegel, W., van der Schrier, G., Andreu-Hayles, L., Baillie, M., Baitinger, C., Bleicher, N., Bonde, N., Brown, D., Carrer, M., Cooper, R., Cufar, K., Dittmar, C., Esper, J., Griggs, C., Gunnarson, B., Günther, B., Gutierrez, E., Haneca, K., Helama, S., Herzig, F., Heussner, K.-U., Hofmann, J., Janda, P., Kontic, R., Köse, N., Kyncl, T., Levanič, T., Linderholm, H., Manning, S., Melvin, T. M., Miles, D., Neuwirth, B., Nicolussi, K., Nola, P., Panayotov, M., Popa, I., Rothe, A., Seftigen, K., Seim, A., Svarva, H., Svoboda, M., Thun, T., Timonen, M., Touchan, R., Trotsiuk, V., Trouet, V., Walder, F., Wazny, T., Wilson, R., and Zang, C.: Old World megadroughts and pluvials during the Common Era, *Sci. Adv.*, 1, e1500561, <https://doi.org/10.1126/sciadv.1500561>, 2015.
- D'Arrigo, R. D. and Wilson, R.: On the Asian expression of the PDO, *Int. J. Climatol.*, 26, 1607–1617, <https://doi.org/10.1002/joc.1326>, 2006.
- D'Arrigo, R. D., Villalba, R., and Wiles, G.: Tree-ring estimates of Pacific decadal climate variability, *Clim. Dynam.*, 18, 219–224, <https://doi.org/10.1007/s003820100177>, 2001.
- Day, J. A., Fung, I. Y., and Risi, C.: Coupling of South and East Asian Monsoon Precipitation in July–August, *J. Climate*, 28, 4330–4356, <https://doi.org/10.1175/JCLI-D-14-00393.1>, 2015.
- Ding, Y., Wang, Z., and Sun, Y.: Inter-decadal variation of the summer precipitation in East China and its association with decreasing Asian summer monsoon. Part I: Observed evidences, *Int. J. Climatol.*, 28, 1139–1161, <https://doi.org/10.1002/joc.1615>, 2008.
- Ding, Y., Sun, Y., Wang, Z., Zhu, Y., and Song, Y.: Inter-decadal variation of the summer precipitation in China and its association with decreasing Asian summer monsoon Part II: Possible causes, *Int. J. Climatol.*, 29, 1926–1944, <https://doi.org/10.1002/joc.1759>, 2009.
- Dufresne, J.-L., Foujols, M.-A., Denvil, S., Caubel, A., Marti, O., Aumont, O., Balkanski, Y., Bekki, S., Bellenger, H., and Benschila, R.: Climate change projections using the IPSL-CM5 Earth System Model: from CMIP3 to CMIP5, *Clim. Dynam.*, 40, 2123–2165, <https://doi.org/10.1007/s00382-012-1636-1>, 2013.
- Evans, M., Kaplan, A., Cane, M., and Villalba, R.: Chapter 4 – Globality and optimality in climate field reconstructions from proxy data, in: *Interhemispheric climate linkages*, ed. Vera Markgraf, Academic Press, San Diego, 53–72, <https://doi.org/10.1016/B978-012472670-3/50007-0>, 2001.
- Feng, J., Li, J. P., Zheng, F., and Sun, C.: Contrasting impacts of developing phases of two types of El Niño on southern China rainfall, *J. Meteorol. Soc. Jpn.*, 94, 359–370, <https://doi.org/10.2151/jmsj.2016-019>, 2016.
- Feng, S., Hu, Q., Wu, Q., and Mann, M. E.: A gridded reconstruction of warm season precipitation for Asia spanning the past half millennium, *J. Climate*, 26, 2192–2204, <https://doi.org/10.1175/jcli-d-12-00099.1>, 2013.
- Fritts, H. C.: *Tree rings and climate*, Academic Press, London, 1976.
- Ge, Q.: *The climate change in China during the past dynasties*, Science Press, Beijing, 2011 (in Chinese).
- Ge, Q., Zheng, J., Hao, Z., Liu, Y., and Li, M.: Recent advances on reconstruction of climate and extreme events in China for the past 2000 years, *J. Geogr. Sci.*, 26, 827–854, <https://doi.org/10.1007/s11442-016-1301-4>, 2016.
- Gómez-Navarro, J. J., Werner, J., Wagner, S., Luterbacher, J., and Zorita, E.: Establishing the skill of climate field reconstruction techniques for precipitation with pseudoproxy experiments, *Clim. Dynam.*, 45, 1395–1413, <https://doi.org/10.1007/s00382-014-2388-x>, 2015.
- Guo, Y., Li, J., and Li, Y.: A time-scale decomposition approach to statistically downscale summer rainfall over North China, *J. Climate*, 25, 572–591, <https://doi.org/10.1175/JCLI-D-11-00014.1>, 2012.
- Hakim, G. J., Emile-Geay, J., Steig, E. J., Noone, D., Anderson, D. M., Tardif, R., Steiger, N., and Perkins, W. A.: The last millennium climate reanalysis project: Framework and first results, *J. Geophys. Res.-Atmos.*, 121, 6745–6764, <https://doi.org/10.1002/2016JD024751>, 2016.
- Hanhijärvi, S., Tingley, M., and Korhola, A.: Pairwise comparisons to reconstruct mean temperature in the Arctic Atlantic Region over the last 2,000 years, *Clim. Dynam.*, 41, 2039–2060, <https://doi.org/10.1007/s00382-013-1701-4>, 2013.
- Hao, Z., Zheng, J., Zhang, X., Liu, H., Li, M., and Ge, Q.: Spatial patterns of precipitation anomalies in eastern China during centennial cold and warm periods of the past 2000 years, *Int. J. Climatol.*, 36, 467–475, <https://doi.org/10.1002/joc.4367>, 2016.
- Hirota, N. and Takahashi, M.: A tripolar pattern as an internal mode of the East Asian summer monsoon, *Clim. Dynam.*, 39, 2219–2238, <https://doi.org/10.1007/s00382-012-1416-y>, 2012.
- Huang, R. and Li, W.: Influence of heat source anomaly over the western tropical Pacific on the subtropical high over East Asia during summer and its physical mechanism, *Chin. J. Atmos. Sci.*, 107–117, 1988 (in Chinese).
- Huang, R. and Wu, Y.: The influence of ENSO on the summer climate change in China and its mechanism, *Adv. Atmos. Sci.*, 6, 21–32, <https://doi.org/10.1007/BF02656915>, 1989.
- Huang, N. and Wu, Z.: A review on Hilbert-Huang transform: method and its applications to geophysical studies, *Rev. Geophys.*, 46, RG2006, <https://doi.org/10.1029/2007RG000228>, 2008.
- Huang, R., Xu, Y., and Zhou, L.: The interdecadal variation of summer precipitations in China and the drought trend in North China, *Plateau Meteorol.*, 18, 465–476, 1999 (in Chinese).
- Jungclauss, J. H., Lorenz, S. J., Timmreck, C., Reick, C. H., Brovkin, V., Six, K., Segschneider, J., Giorgetta, M. A., Crowley, T. J., Pongratz, J., Krivova, N. A., Vieira, L. E., Solanki, S. K., Klocke, D., Botzet, M., Esch, M., Gayler, V., Haak, H., Radatz, T. J., Roeckner, E., Schnur, R., Widmann, H., Claussen, M., Stevens, B., and Marotzke, J.: Climate and carbon-cycle variability over the last millennium, *Clim. Past*, 6, 723–737, <https://doi.org/10.5194/cp-6-723-2010>, 2010.

- Kang, S., Bräuning, A., and Ge, H.: Tree-ring based evidence of the multi-decadal climatic oscillation during the past 200 years in north-central China, *J. Arid Environ.*, 110, 53–59, <https://doi.org/10.1016/j.jaridenv.2014.06.003>, 2014.
- Karori, M. A., Li, J., and Jin, F.: The asymmetric influence of the two types of El Niño and La Niña on summer rainfall over Southeast China, *J. Climate*, 26, 4567–4582, <https://doi.org/10.1175/JCLI-D-12-00324.1>, 2013.
- Klein, F., Goosse, H., Graham, N. E., and Verschuren, D.: Comparison of simulated and reconstructed variations in East African hydroclimate over the last millennium, *Clim. Past*, 12, 1499–1518, <https://doi.org/10.5194/cp-12-1499-2016>, 2016.
- Landrum, L., Otto-Bliesner, B. L., Wahl, E. R., Conley, A., Lawrence, P. J., Rosenbloom, N., and Teng, H.: Last millennium climate and its variability in CCSM4, *J. Climate*, 26, 1085–1111, <https://doi.org/10.1175/JCLI-D-11-00326.1>, 2012.
- Li, J., Xie, S., Cook, E. R., Morales, M. S., Christie, D. A., Johnson, N. C., Chen, F., D’Arrigo, R. D., Fowler, A. M., Gou, X., and Fang, K.: El Niño modulations over the past seven centuries, *Nat. Clim. Change*, 3, 822–826, <https://doi.org/10.1038/nclimate1936>, 2013a.
- Li, J., Ren, R., Qi, Y., Wang, F., Lu, R., Zhang, P., Jiang, Z., Duan, W., Yu, F., and Yang, Y.: Progress in air-land-sea interactions in Asia and their role in global and Asian climate change, *Chin. J. Atmos. Sci.*, 37, 518–538, 2013b (in Chinese).
- Li, Q., Peng, J., and Shen, Y.: Development of China homogenized monthly precipitation dataset during 1900–2009, *J. Geogr. Sci.*, 22, 579–593, <https://doi.org/10.1007/s11442-012-0948-8>, 2012.
- Li, Z., Lau, W. K. M., Ramanathan, V., Wu, G., Ding, Y., Manoj, M. G., Liu, J., Qian, Y., Li, J., Zhou, T., Fan, J., Rosenfeld, D., Ming, Y., Wang, Y., Huang, J., Wang, B., Xu, X., Lee, S. S., Cribb, M., Zhang, F., Yang, X., Zhao, C., Takemura, T., Wang, K., Xia, X., Yin, Y., Zhang, H., Guo, J., Zhai, P. M., Sugimoto, N., Babu, S. S., and Brasseur, G. P.: Aerosol and monsoon climate interactions over Asia, *Rev. Geophys.*, 54, 866–929, <https://doi.org/10.1002/2015RG000500>, 2016.
- Liu, F., Chai, J., Wang, B., Liu, J., Zhang, X., and Wang, Z.: Global monsoon precipitation responses to large volcanic eruptions, *Sci. Rep.*, 6, 24331, <https://doi.org/10.1038/srep24331>, 2016.
- Luterbacher, J., Dietrich, D., Xoplaki, E., Grosjean, M., and Wanner, H.: European seasonal and annual temperature variability, trends, and extremes since 1500, *Science*, 303, 1499–1503, <https://doi.org/10.1126/science.1093877>, 2004.
- Ma, Z.: The interdecadal trend and shift of dry/wet over the central part of North China and their relationship to the Pacific Decadal Oscillation (PDO), *Chinese Sci. Bull.*, 52, 2130–2139, <https://doi.org/10.1007/s11434-007-0284-z>, 2007.
- Man, W., Zhou, T., and Jungclaus, J. H.: Effects of large volcanic eruptions on global summer climate and East Asian monsoon changes during the Last millennium: Analysis of MPI-ESM simulations, *J. Climate*, 27, 7394–7409, <https://doi.org/10.1175/JCLI-D-13-00739.1>, 2014.
- Man, Z.: Climatic change historical period of China, Shandong Education Press, Jinan, 2009 (in Chinese).
- Mann, M. E., Park, J., and Bradley, R.: Global interdecadal and century-scale climate oscillations during the past five centuries, *Nature*, 378, 266–270, <https://doi.org/10.1038/378266a0>, 1995.
- Mann, M. E., Bradley, R. S., and Hughes, M. K.: Northern hemisphere temperatures during the past millennium: Inferences, uncertainties, and limitations, *Geophys. Res. Lett.*, 26, 759–762, <https://doi.org/10.1029/1999GL900070>, 1999.
- Mann, M. E., Zhang, Z., Hughes, M. K., Bradley, R. S., Miller, S. K., Rutherford, S., and Ni, F.: Proxy-based reconstructions of hemispheric and global surface temperature variations over the past two millennia, *P. Natl. Acad. Sci. USA*, 105, 13252–13257, <https://doi.org/10.1073/pnas.0805721105>, 2008.
- Mann, M. E., Zhang, Z. H., Rutherford, S., Bradley, R. S., Hughes, M. K., Shindell, D., Ammann, C., Faluvegi, G., and Ni, F. B.: Global Signatures and Dynamical Origins of the Little Ice Age and Medieval Climate Anomaly, *Science*, 326, 1256–1260, <https://doi.org/10.1126/science.1177303>, 2009.
- McGregor, S., Timmermann, A., and Timm, O.: A unified proxy for ENSO and PDO variability since 1650, *Clim. Past*, 6, 1–17, <https://doi.org/10.5194/cp-6-1-2010>, 2010.
- McShane, B. B. and Wyner, A. J.: A statistical analysis of multiple temperature proxies: Are reconstructions of surface temperatures over the last 1000 years reliable?, *Ann. Appl. Stat.*, 5, 5–44, <https://doi.org/10.1214/10-AOAS398>, 2011.
- Neukom, R., Luterbacher, J., Villalba, R., Kuttel, M., Frank, D., Jones, P. D., Grosjean, M., Wanner, H., Aravena, J. C., Black, D. E., Christie, D. A., D’Arrigo, R. D., Lara, A., Morales, M., Soliz-Gamboa, C., Srur, A., Urrutia, R., and von Gunten, L.: Multiproxy summer and winter surface air temperature field reconstructions for southern South America covering the past centuries, *Clim. Dynam.*, 37, 35–51, <https://doi.org/10.1007/s00382-010-0793-3>, 2011.
- Neukom, R., Nash, D. J., Endfield, G. H., Grab, S. W., Grove, C. A., Kelso, C., Vogel, C. H., and Zinke, J.: Multi-proxy summer and winter precipitation reconstruction for southern Africa over the last 200 years, *Clim. Dynam.*, 42, 2713–2726, <https://doi.org/10.1007/s00382-013-1886-6>, 2013.
- Newman, M., Alexander, M. A., Ault, T. R., Cobb, K. M., Deser, C., Di Lorenzo, E., Mantua, N. J., Miller, A. J., Minobe, S., and Nakamura, H.: The Pacific decadal oscillation, revisited, *J. Climate*, 29, 4399–4427, <https://doi.org/10.1175/JCLI-D-15-0508.1>, 2016.
- Nitta, T.: Convective activities in the tropical western Pacific and their impact on the Northern Hemisphere summer circulation, *J. Meteorol. Soc. Jpn.*, 65, 373–390, https://doi.org/10.2151/jmsj1965.65.3_373, 1987.
- North, G. R., Bell, T. L., Cahalan, R. F., and Moeng, F. J.: Sampling errors in the estimation of empirical orthogonal functions, *Mon. Weather Rev.*, 110, 699–706, [https://doi.org/10.1175/1520-0493\(1982\)110<0699:SEITEO>2.0.CO;2](https://doi.org/10.1175/1520-0493(1982)110<0699:SEITEO>2.0.CO;2), 1982.
- PAGES 2k Consortium: Continental-scale temperature variability during the past two millennia, *Nat. Geosci.*, 6, 339–346, <https://doi.org/10.1038/ngeo1797>, 2013.
- PAGES 2k Consortium: A global multiproxy database for temperature reconstructions of the Common Era, *Sci. Data*, 4, 170088, <https://doi.org/10.1038/sdata.2017.88>, 2017.
- Palmer, J. G., Cook, E. R., Turney, C. S., Allen, K., Fenwick, P., Cook, B. I., O’Donnell, A., Lough, J., Grierson, P., and Baker, P.: Drought variability in the eastern Australia and New Zealand summer drought atlas (ANZDA, CE 1500–2012) modulated by the Interdecadal Pacific Oscillation, *Environ. Res. Lett.*, 10, 124002, <https://doi.org/10.1088/1748-9326/10/12/124002>, 2015.
- Pei, L., Yan, Z., and Hui, Y.: Multidecadal variability of dry/wet patterns in eastern China and their relationship with the Pacific

- Decadal Oscillation in the last 413 years, *Chinese Sci. Bull.*, 60, 97–108, <https://doi.org/10.1360/n972014-00790>, 2015.
- Qian, C. and Zhou, T.: Multidecadal variability of North China aridity and its relationship to PDO during 1900–2010, *J. Climate*, 27, 1210–1222, <https://doi.org/10.1175/JCLI-D-13-00235.1>, 2014.
- Qian, W., Hu, Q., Zhu, Y., and Lee, D.: Centennial-scale dry-wet variations in East Asia, *Clim. Dynam.*, 21, 77–89, <https://doi.org/10.1007/s00382-003-0319-3>, 2003a.
- Qian, W., Chen, D., Zhu, Y., and Shen, H.: Temporal and spatial variability of dryness/wetness in China during the last 530 years, *Theor. Appl. Climatol.*, 76, 13–29, <https://doi.org/10.1007/s00704-003-0009-4>, 2003b.
- Ruan, C. and Li, J.: An improvement in a time-scale decomposition statistical downscaling prediction model for summer rainfall over North China, *Chin. J. Atmos. Sci.*, 40, 215–226, <https://doi.org/10.3878/j.issn.1006-9895.1503.14317>, 2016 (in Chinese).
- Schmidt, G. A., Kelley, M., Nazarenko, L., Ruedy, R., Russell, G. L., Aleinov, I., Bauer, M., Bauer, S. E., Bhat, M. K., and Bleck, R.: Configuration and assessment of the GISS ModelE2 contributions to the CMIP5 archive, *J. Adv. Model. Earth Sy.*, 6, 141–184, <https://doi.org/10.1002/2013MS000265>, 2014.
- Schneider, T.: Analysis of incomplete climate data: Estimation of mean values and covariance matrices and imputation of missing values, *J. Climate*, 14, 853–871, [https://doi.org/10.1175/1520-0442\(2001\)014<0853:AOICDE>2.0.CO;2](https://doi.org/10.1175/1520-0442(2001)014<0853:AOICDE>2.0.CO;2), 2001.
- Schubert, S. D., Stewart, R. E., Wang, H., Barlow, M., Berbery, E. H., Cai, W., Hoerling, M. P., Kanikicharla, K. K., Koster, R. D., and Lyon, B.: Global meteorological drought: A synthesis of current understanding with a focus on SST drivers of precipitation deficits, *J. Climate*, 29, 3989–4019, <https://doi.org/10.1175/JCLI-D-15-0452.1>, 2016.
- Seftigen, K., Björklund, J., Cook, E., and Linderholm, H.: A tree-ring field reconstruction of Fennoscandian summer hydroclimate variability for the last millennium, *Clim. Dynam.*, 44, 3141–3154, <https://doi.org/10.1007/s00382-014-2191-8>, 2015.
- Shao, X., Huang, L., Liu, H., Liang, E., Fang, X., and Wang, L.: Reconstruction of precipitation variation from tree rings in recent 1000 years in Delingha, Qinghai, *Sci. China Ser. D*, 48, 939–949, <https://doi.org/10.1360/03yd0146>, 2005.
- Shen, C., Wang, W. C., Gong, W., and Hao, Z.: A Pacific Decadal Oscillation record since 1470 AD reconstructed from proxy data of summer rainfall over eastern China, *Geophys. Res. Lett.*, 33, L03702, <https://doi.org/10.1029/2005GL024804>, 2006.
- Shi, F., Yang, B., Ljungqvist, F. C., and Yang, F.: Multi-proxy reconstruction of Arctic summer temperatures over the past 1400 years, *Clim. Res.*, 54, 113–128, <https://doi.org/10.3354/cr01112>, 2012.
- Shi, F., Li, J., and Wilson, R.: A tree-ring reconstruction of the South Asian summer monsoon index over the past millennium, *Sci. Rep.-UK*, 4, 6739, <https://doi.org/10.1038/srep06739>, 2014.
- Shi, F., Ge, Q., Yang, B., Li, J., Yang, F., Ljungqvist, F. C., Solomina, O., Nakatsuka, T., Wang, N., Zhao, S., Xu, C., Fang, K., Sano, M., Chu, G., Fan, Z., Gaire, N. P., and Zafar, M. U.: A multi-proxy reconstruction of spatial and temporal variations in Asian summer temperatures over the last millennium, *Climatic Change*, 131, 663–676, <https://doi.org/10.1007/s10584-015-1413-3>, 2015a.
- Shi, F., Yang, B., Feng, J., Li, J., Yang, F., and Guo, Z.: Reconstruction of the Northern Hemisphere annual temperature change over the common era derived from tree rings, *Quaternary Sci.*, 35, 1051–1063, <https://doi.org/10.11928/j.issn.1001-7410.2015.05.01>, 2015b (in Chinese).
- Shi, F., Fang, K., Xu, C., Guo, Z., and Borgaonkar, H. P.: Interannual to centennial variability of the South Asian summer monsoon over the past millennium, *Clim. Dynam.*, 49, 2803–2814, <https://doi.org/10.1007/s00382-016-3493-9>, 2017.
- Shi, Z., Xu, T., and Wang, H.: Sensitivity of Asian climate change to radiative forcing during the last millennium in a multi-model analysis, *Global Planet. Change*, 139, 195–210, <https://doi.org/10.1016/j.gloplacha.2016.02.007>, 2016.
- Sigl, M., Winstrup, M., McConnell, J. R., Welten, K. C., Plunkett, G., Ludlow, F., Buntgen, U., Caffee, M., Chellman, N., Dahl-Jensen, D., Fischer, H., Kipfsthuhl, S., Kostick, C., Maselli, O. J., Mekhaldi, F., Mulvaney, R., Muscheler, R., Pasteris, D. R., Pilcher, J. R., Salzer, M., Schupbach, S., Steffensen, J. P., Vinther, B. M., and Woodruff, T. E.: Timing and climate forcing of volcanic eruptions for the past 2,500 years, *Nature*, 523, 543–549, <https://doi.org/10.1038/nature14565>, 2015.
- Song, F. and Zhou, T.: The crucial role of internal variability in modulating the decadal variation of the East Asian summer monsoon – ENSO relationship during the twentieth century, *J. Climate*, 28, 7093–7107, <https://doi.org/10.1175/JCLI-D-14-00783.1>, 2015.
- Stuecker, M. F., Timmermann, A., Jin, F., McGregor, S., and Ren, H.-L.: A combination mode of the annual cycle and the El Niño/Southern Oscillation, *Nat. Geosci.*, 6, 540–544, <https://doi.org/10.1038/ngeo1826>, 2013.
- Tingley, M. P. and Huybers, P.: A Bayesian Algorithm for Reconstructing Climate Anomalies in Space and Time. Part I: Development and Applications to Paleoclimate Reconstruction Problems, *J. Climate*, 23, 2759–2781, <https://doi.org/10.1175/2009jcli3015.1>, 2010.
- Wan, H., Zhang, X., Zwiers, F. W., and Shiogama, H.: Effect of data coverage on the estimation of mean and variability of precipitation at global and regional scales, *J. Geophys. Res.-Atmos.*, 118, 534–546, <https://doi.org/10.1002/jgrd.50118>, 2013.
- Wang, B., Wu, R., and Fu, X.: Pacific–east Asian teleconnection: How does ENSO affect east Asian climate?, *J. Climate*, 13, 1517–1536, [https://doi.org/10.1175/1520-0442\(2000\)013<1517:PEATHD>2.0.CO;2](https://doi.org/10.1175/1520-0442(2000)013<1517:PEATHD>2.0.CO;2), 2000.
- Wang, S. and Zhao, Z.: An analyses of historical data of droughts and floods in last 500 years in China, *Acta Geol. Sin.*, 34, 329–341, 1979 (in Chinese).
- Wang, S., Gong, D., and Zhu, J.: Twentieth-century climatic warming in China in the context of the Holocene, *Holocene*, 11, 313–321, <https://doi.org/10.1191/095968301673172698>, 2001.
- Wang, S., Cai, J., Mu, Q., Xie, Z., and Dong, W.: Climate change of annual precipitation in western China, *J. Nat. Resour.*, 17, 415–422, 2002 (in Chinese).
- Wang, Y., Lean, J. L., and Sheeley, N. R.: Modeling the sun’s magnetic field and irradiance since 1713, *Astrophys. J.*, 625, 522–538, <https://doi.org/10.1086/429689>, 2005.
- Widmann, M., Goosse, H., van der Schrier, G., Schnur, R., and Barkmeijer, J.: Using data assimilation to study extratropical Northern Hemisphere climate over the last millennium, *Clim. Past*, 6, 627–644, <https://doi.org/10.5194/cp-6-627-2010>, 2010.

- Wu, B., Li, T., and Zhou, T.: Relative contributions of the Indian Ocean and local SST anomalies to the maintenance of the Western North Pacific anomalous anticyclone during the El Niño decaying summer, *J. Climate*, 23, 2974–2986, <https://doi.org/10.1175/2010JCLI3300.1>, 2010.
- Wu, R. and Wang, B.: A Contrast of the East Asian Summer Monsoon–ENSO Relationship between 1962–77 and 1978–93, *J. Climate*, 15, 3266–3279, [https://doi.org/10.1175/1520-0442\(2002\)015<3266:ACOTEA>2.0.CO;2](https://doi.org/10.1175/1520-0442(2002)015<3266:ACOTEA>2.0.CO;2), 2002.
- Wu, T., Yu, R., Zhang, F., Wang, Z., Dong, M., Wang, L., Jin, X., Chen, D., and Li, L.: The Beijing Climate Center atmospheric general circulation model: description and its performance for the present-day climate, *Clim. Dynam.*, 34, 123–147, <https://doi.org/10.1007/s00382-008-0487-2>, 2010.
- Wu, Z. and Huang, N.: Ensemble empirical mode decomposition: a noise assisted data analysis method, *Adv. Adapt. Data Anal.*, 1, 1–41, <https://doi.org/10.1142/S1793536909000047>, 2009.
- Wu, Z., Wang, B., Li, J., and Jin, F.: An empirical seasonal prediction model of the East Asian summer monsoon using ENSO and NAO, *J. Geophys. Res.-Atmos.*, 114, D18120, <https://doi.org/10.1029/2009JD011733>, 2009.
- Wu, Z., Li, J., Jiang, Z., and Ma, T.: Modulation of the Tibetan Plateau snow cover on the ENSO teleconnections: From the East Asian summer monsoon perspective, *J. Climate*, 25, 2481–2489, <https://doi.org/10.1175/JCLI-D-11-00135.1>, 2012.
- Xie, S., Hu, K., Hafner, J., Tokinaga, H., Du, Y., Huang, G., and Sampe, T.: Indian Ocean capacitor effect on Indo-western Pacific climate during the summer following El Niño, *J. Climate*, 22, 730–747, <https://doi.org/10.1175/2008JCLI2544.1>, 2009.
- Yang, B., Kang, S., Ljungqvist, F. C., He, M., Zhao, Y., and Qin, C.: Drought variability at the northern fringe of the Asian summer monsoon region over the past millennia, *Clim. Dynam.*, 43, 845–859, <https://doi.org/10.1007/s00382-013-1962-y>, 2014a.
- Yang, B., Qin, C., Wang, J., He, M., Melvin, T. M., Osborn, T. J., and Briffa, K. R.: A 3,500-year tree-ring record of annual precipitation on the northeastern Tibetan Plateau, *P. Natl. Acad. Sci. USA*, 111, 2903–2908, <https://doi.org/10.1073/pnas.1319238111>, 2014b.
- Yang, F., Shi, F., Kang, S., Wang, S., Xiao, Z., Nakatsuka, T., and Shi, J.: Comparison of the dryness/wetness index in China with the Monsoon Asia Drought Atlas, *Theor. Appl. Climatol.*, 114, 553–566, <https://doi.org/10.1007/s00704-013-0858-4>, 2013a.
- Yang, F., Wang, N., Shi, F., Ljungqvist, F. C., Wang, S., Fan, Z., and Lu, J.: Multi-proxy temperature reconstruction from the West Qinling Mountains, China, for the past 500 years, *PLoS ONE*, 8, e57638, <https://doi.org/10.1371/journal.pone.0057638>, 2013b.
- Yang, F., Wang, N., Shi, F., Ljungqvist, F. C., Zhao, S., and Liu, T.: The spatial distribution of precipitation over the West Qinling region, China, AD 1470–2000, *Palaeogeogr. Palaeoclimatol.*, 443, 278–285, <https://doi.org/10.1016/j.palaeo.2015.12.003>, 2016.
- Yu, R. and Zhou, T.: Seasonality and three-dimensional structure of interdecadal change in the East Asian monsoon, *J. Climate*, 20, 5344–5355, <https://doi.org/10.1175/2007JCLI1559.1>, 2007.
- Zhang, D.: Method to reconstruct climatic series for the past 500 years and its reliability, *Collected Papers of Meteorological Science and Technology*, 4, 17–26, 1983 (in Chinese).
- Zhang, D.: The method for reconstruction of the dryness/wetness series in China for the last 500 years and its reliability, in: *The reconstruction of climate in China for historical times*, edited by: Zhang, J., Science Press, Beijing, China, 18–30, 1988.
- Zhang, D.: Historical records of climate change in China, *Quaternary Sci. Rev.*, 10, 551–554, [https://doi.org/10.1016/0277-3791\(91\)90049-Z](https://doi.org/10.1016/0277-3791(91)90049-Z), 1991.
- Zhang, D.: A compendium of Chinese meteorological records of the last 3000 years, Jiangsu Education Publishing House, Nanjing, 2004 (in Chinese).
- Zhang, D.: Test of calibration on the paleoclimatic proxy data by using Chinese historical records, *Adv. Climate Change Res.*, 6, 70–72, <https://doi.org/10.3724/SP.J.1248.2011.00038>, 2010.
- Zhang, D. and Liu, C.: Continuation (1980–1992) of the yearly charts of dryness/wetness in China for the last 500 years period, *Meteor. Mon.*, 19, 41–45, 1993 (in Chinese).
- Zhang, D., Li, X., and Liang, Y.: Continuation (1992–2000) of the yearly charts of dryness/wetness in China for the last 500 years period, *J. Appl. Meteorol. Sci.*, 14, 379–384, 2003a (in Chinese).
- Zhang, D., Wang, L., and Sun, X.: Reconstruction of grid precipitation anomaly in Eastern China from historical documents: New study on Chinese historical climate records, *Quaternary Sci.*, 23, 177–184, 2003b (in Chinese).
- Zhang, L. and Zhou, T.: Drought over East Asia: A Review, *J. Climate*, 28, 3375–3399, <https://doi.org/10.1175/JCLI-D-14-00259.1>, 2015.
- Zhang, Q., Cheng, G., Yao, T., Kang, X., and Huang, J.: A 2,326-year tree-ring record of climate variability on the northeastern Qinghai-Tibetan Plateau, *Geophys. Res. Lett.*, 30, 1739–1742, <https://doi.org/10.1029/2003gl017425>, 2003.
- Zhang, W., Jin, F., Li, J., and Ren, H.: Contrasting impacts of two-type El Niño over the western North Pacific during boreal autumn, *J. Meteorol. Soc. Jpn.*, 89, 563–569, <https://doi.org/10.2151/jmsj.2011-510>, 2011.
- Zhang, W., Jin, F., Stuecker, M. F., Wittenberg, A. T., Timmermann, A., Ren, H. L., Kug, J. S., Cai, W., and Cane, M.: Unraveling El Niño’s impact on the East Asian Monsoon and Yangtze River summer flooding, *Geophys. Res. Lett.*, 43, 11,375–11,382, <https://doi.org/10.1002/2016GL071190>, 2016.
- Zhao, S., Li, J., and Sun, C.: Decadal variability in the occurrence of wintertime haze in central eastern China tied to the Pacific Decadal Oscillation, *Sci. Rep.-UK*, 6, 27424, <https://doi.org/10.1038/srep27424>, 2016.
- Zhao, Y. and Zhu, J.: Assessing quality of grid daily precipitation datasets in China in recent 50 years, *Plateau Meteorol.*, 34, 50–58, 2015 (in Chinese).
- Zheng, F., Li, J., Li, Y., Zhao, S., and Deng, D.: Influence of the summer NAO on the spring-NAO-based predictability of the East Asian summer monsoon, *J. Appl. Meteorol. Clim.*, 55, 1459–1476, <https://doi.org/10.1175/JAMC-D-15-0199.1>, 2016.
- Zheng, J., Wang, W., Ge, Q., Man, Z., and Zhang, P.: Precipitation variability and extreme events in eastern China during the past 1500 years, *Terr. Atmos. Ocean. Sci.*, 17, 579–592, [https://doi.org/10.3319/TAO.2006.17.3.579\(A\)](https://doi.org/10.3319/TAO.2006.17.3.579(A)), 2006.
- Zheng, J., Ge, Q., Hao, Z., Liu, H., Man, Z., Hou, Y., and Fang, X.: Paleoclimatology proxy recorded in historical documents and method for reconstruction on climate change, *Quaternary Sci.*, 34, 1186–1196, <https://doi.org/10.3969/j.issn.1001-7410.2014.06.07>, 2014a (in Chinese).
- Zheng, J., Hao, Z., Fang, X., and Ge, Q.: Changing characteristics of extreme climate events during past 2000 years in China, *Prog.*

- Geogr., 33, 3–12, <https://doi.org/10.11820/dlkxjz.2014.01.001>, 2014b (in Chinese).
- Zhou, T., Gong, D., Li, J., and Li, B.: Detecting and understanding the multi-decadal variability of the East Asian summer monsoon recent progress and state of affairs, *Meteorol. Z.*, 18, 455–467, <https://doi.org/10.1127/0941-2948/2009/0396>, 2009.
- Zhuo, Z., Gao, C., and Pan, Y.: Proxy evidence for China's monsoon precipitation response to volcanic aerosols over the past seven centuries, *J. Geophys. Res.-Atmos.*, 119, 6638–6652, <https://doi.org/10.1002/2013JD021061>, 2014.